

Solubility and stability of liebigite, $\text{Ca}_2\text{UO}_2(\text{CO}_3)_3 \cdot 10\text{H}_2\text{O}(\text{cr})$, in dilute to concentrated NaCl and NaClO_4 solutions at $T = 22\text{--}80\text{ }^\circ\text{C}$

J.-Y. Lee^{a,b,**}, S. Amayri^c, V. Montoya^{a,1}, D. Fellhauer^a, X. Gaona^{a,*}, M. Altmaier^a

^a Karlsruhe Institute of Technology, Institute for Nuclear Waste Disposal, P.O. Box 3640, 76021, Karlsruhe, Germany

^b Pusan National University, School of Mechanical Engineering, 2, Busandaehak-ro 63beon-gil, Geunjeong-gu, Busan, Republic of Korea

^c Johannes Gutenberg University Mainz, Institute of Nuclear Chemistry, Fritz-Strassmann-Weg 2, 55099, Mainz, Germany

ARTICLE INFO

Editorial handling by Jon Petter Gustafsson

Keywords:

Uranium

Liebigite

Andersonite

Solubility

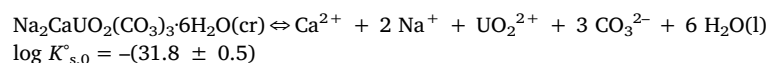
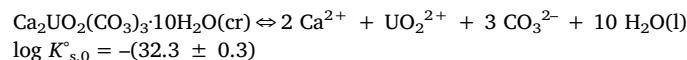
Thermodynamics

Elevated temperature

ABSTRACT

The solubility and thermodynamic stability of a synthetic liebigite was investigated in NaCl and NaClO_4 solutions within a wide range of ionic strength ($0.03\text{ m} \leq I_m \leq 5.61\text{ m}$), pH ($7 \leq \text{pH}_m \leq 9$, with $\text{pH}_m = -\log[\text{H}^+]$) and temperature ($22\text{ }^\circ\text{C} \leq T \leq 80\text{ }^\circ\text{C}$) conditions. A comprehensive characterization of the synthetic solid phase using XRD, quantitative chemical analysis, TG-DTA, SEM-EDS, IR and Raman spectroscopy confirmed the stoichiometry of $\text{Ca}_2\text{UO}_2(\text{CO}_3)_3 \cdot 10\text{H}_2\text{O}(\text{cr})$. At room temperature, liebigite remains stable and controls the solubility of U(VI) in the investigated NaCl and NaClO_4 systems with $I_m \leq 0.51\text{ m}$. For the same temperature but high ionic strength (5.61 m NaCl), liebigite transforms into andersonite ($\text{Na}_2\text{CaUO}_2(\text{CO}_3)_3 \cdot 6\text{H}_2\text{O}(\text{cr})$). This solid phase transformation results in a decrease in solubility of approximately 2 \log_{10} -units at $\text{pH}_m \approx 8$. Solubility data in combination with solid phase characterization (XRD, quantitative chemical analysis) likewise confirm the transformation of liebigite into $\text{CaU}_2\text{O}_7 \cdot x\text{H}_2\text{O}(\text{cr})$, $\text{Na}_2\text{U}_2\text{O}_7 \cdot x\text{H}_2\text{O}(\text{cr})$ and/or other sub-stoichiometric Na-uranate compounds in all systems investigated at $T = 80\text{ }^\circ\text{C}$.

On the basis of solubility data at room temperature determined in this work, in combination with thermodynamic and activity models available in the literature for the aqueous speciation in the system Ca–U(VI)–carbonate, solubility products for liebigite and andersonite are derived:



These results complement previously reported thermodynamic data, now allowing complete thermodynamic and geochemical calculations for the system $\text{UO}_2^{2+}\text{--Ca}^{2+}\text{--Na}^+\text{--H}^+\text{--CO}_2(\text{g})\text{--HCO}_3^-\text{--CO}_3^{2-}\text{--H}_2\text{O}(\text{l})$, including U(VI) aqueous species and solid compounds, in the context of environmental uranium chemistry and nuclear waste disposal.

1. Introduction

Uranium is an important actinide element in the context of nuclear waste disposal mostly due to its large inventory in high-level radioactive waste and its redox-sensitive character, which can lead to important changes in its chemical behavior with the alteration of the redox boundary conditions. Although uranium is expected to be present

as U(IV) under the very reducing conditions foreseen in deep underground repositories (Guillaumont et al., 2003), the oxidation to U(VI) with the consequent increase in solubility can be promoted under specific boundary conditions, e.g. intense radiolytic field, contact with an oxidizing plume (e.g. nitrate), presence of complexing ligands stabilizing U(VI), etc. Carbonate is a ubiquitous component in groundwater, and it is expected in moderate concentrations (1–10 mM) in the

* Corresponding author.

** Corresponding author. Karlsruhe Institute of Technology, Institute for Nuclear Waste Disposal, P.O. Box 3640, 76021, Karlsruhe, Germany.

E-mail addresses: jylee@pusan.ac.kr (J.-Y. Lee), xavier.gaona@kit.edu (X. Gaona).

¹ Current address (V. Montoya): Department of Environmental Informatics, Helmholtz Centre for Environmental Research – UFZ, Permoserstr. 15, 04318, Leipzig,

pore- and groundwaters of clay- and crystalline-based repositories for nuclear waste disposal (Choi et al., 2008; Gaucher et al., 2006; Grivé et al., 2010; Olmeda et al., 2017). Although both U(IV) and U(VI) form aqueous complexes with carbonate, more stable U(VI)–carbonate complexes are described to form under near-neutral pH conditions. This is mostly due to the very stable U(VI) moiety " $\text{UO}_2(\text{CO}_3)_3^{4-}$ ", and to the stronger hydrolysis controlling the solution chemistry of U(IV) in this pH-range compared to U(VI) (Altmaier et al., 2017; Çevirim-Papaioannou et al., 2018a, 2018b; Guillaumont et al., 2003). In Ca-containing systems, a large body of experimental studies has provided sound evidence on the formation of very stable ternary complexes Ca–U(VI)–carbonate ($\text{CaUO}_2(\text{CO}_3)_3^{2-}$ and $\text{Ca}_2\text{UO}_2(\text{CO}_3)_3(\text{aq})$) (Bernhard et al., 2001; Dong and Brooks, 2006; Endrizzi and Rao, 2014; Geipel et al., 2008; Lee et al., 2017; Lee and Yun, 2013). These species play also a predominant role in controlling the aquatic chemistry of uranium in marine environments (Beccia et al., 2017; Endrizzi et al., 2016; Maloubier et al., 2015). Furthermore, several experimental studies have been dedicated to investigate the impact of the ternary complexes Ca–U(VI)–carbonate on the sorption properties of U(VI) on clay and granite rock, lacustrine sediments, ferrihydrite, alumina or silica, among other materials (Amayri, 2002; Fox et al., 2006; Jo et al., 2018; Maia et al., 2017; Saleh et al., 2018; Seder-Colomina et al., 2018).

A number of ternary $R[\text{UO}_2(\text{CO}_3)_3] \cdot n\text{H}_2\text{O}$ minerals ($R = \text{Ca}_2$ (liebigite), Na_2Ca (andersonite), Mg_2 (bayleyite) and CaMg (swartzite), with $n = 10, 6, 18$ and 12 , respectively) are observed in nature and have been characterized in the literature, thus reflecting the potential stability of these ternary solid phases (Vochten et al., 1993). In spite of this, the number of experimental studies investigating their solubility and reporting their thermodynamic properties is very limited (Alwan and Williams, 1980; Amayri, 2002; Chernorukov et al., 2009). Alwan and Williams investigated the solubility of liebigite, andersonite, bayleyite and swartzite at $T = 274\text{--}294\text{ K}$ in the absence of $\text{CO}_2(\text{g})$, and reported their solubility constants ($\log K_{s,0}^\circ$), Gibbs energies and enthalpies of formation ($\Delta_f G^\circ$ and $\Delta_f H^\circ$) (Alwan and Williams, 1980). These authors were unaware of the formation of the ternary aqueous complexes $\text{CaUO}_2(\text{CO}_3)_3^{2-}$ and $\text{Ca}_2\text{UO}_2(\text{CO}_3)_3(\text{aq})$, and thus interpreted their solubility data assuming the predominance of binary U(VI)–carbonate complexes in the aqueous phase. The original data reported by Alwan and Williams were later re-evaluated by Gorman-Lewis et al. (2008) and Endrizzi et al. (2016) accounting for the formation of the indicated ternary aqueous species. In his PhD thesis, Amayri synthesized and characterized the solid phases $\text{M}_2[\text{UO}_2(\text{CO}_3)_3] \cdot x\text{H}_2\text{O}(\text{cr})$ with $M = \text{Mg}, \text{Ca}, \text{Sr}$ and Ba (Amayri, 2002). The author also investigated the solubility of these solid phases at $7 \leq \text{pH} \leq 9$, and reported the corresponding solubility constants for the equilibrium reaction $\text{M}_2[\text{UO}_2(\text{CO}_3)_3] \cdot x\text{H}_2\text{O}(\text{cr}) + 3 \text{H}^+ \rightleftharpoons 2 \text{M}^{2+} + \text{UO}_2^{2+} + \text{HCO}_3^- + x \text{H}_2\text{O}(\text{l})$. Chernorukov and co-workers synthesized the solid phases $\text{M}_2[\text{UO}_2(\text{CO}_3)_3] \cdot x\text{H}_2\text{O}(\text{cr})$ with $M = \text{Mg}, \text{Ca}, \text{Sr}$ and Ba , and extensively characterized them by X-Ray Diffraction (XRD), Infrared spectroscopy (IR) and Thermogravimetry – Differential Thermal Analysis (TG–DTA) (Chernorukov et al., 2009). The authors determined the dissolution enthalpy of these solid phases by calorimetric measurements, and reported the corresponding formation enthalpies using the thermochemical cycle $\text{UO}_2\text{CO}_3(\text{cr}) + 2\text{MCO}_3(\text{cr}) + n \text{H}_2\text{O}(\text{l}) \rightleftharpoons \text{M}_2[\text{UO}_2(\text{CO}_3)_3] \cdot n\text{H}_2\text{O}(\text{cr})$.

The ternary solid phases discussed above (especially liebigite and andersonite) can be responsible of controlling the solubility of U(VI) within boundary conditions where the ternary species $\text{MUO}_2(\text{CO}_3)_3^{2-}$ and $\text{M}_2\text{UO}_2(\text{CO}_3)_3(\text{aq})$ prevail in the aqueous phase. Although equilibrium constants for the formation of such ternary aqueous complexes are properly described in the literature, a systematic study investigating the thermodynamic properties of the corresponding solid phases is so far missing. In this context, the present work aims at investigating the solubility and stability of liebigite, $\text{Ca}_2\text{UO}_2(\text{CO}_3)_3 \cdot 10\text{H}_2\text{O}(\text{cr})$, over a broad range of ionic strength ($0.03 \text{ m} \leq I \leq 5.61 \text{ m}$), pH ($7 \leq \text{pH}_m \leq 9$) and temperature ($22^\circ\text{C} \leq T \leq 80^\circ\text{C}$) conditions of potential relevance in the context on nuclear waste disposal (Altmaier et al., 2013, 2017;

Neck et al., 2009). The final goal is to determine the solubility product of $\text{Ca}_2\text{UO}_2(\text{CO}_3)_3 \cdot 10\text{H}_2\text{O}(\text{cr})$ and its temperature dependence, consistently with the state of the art thermodynamics available for the ternary system Ca–U(VI)–carbonate in the aqueous phase.

2. Experimental

2.1. Chemicals

All solutions were prepared with ultrapure water (18.2 MΩ cm, Milli-Q®, Merck Millipore), and were handled under air at $T = 22\text{--}80^\circ\text{C}$ (see description of solubility experiments in Section 2.3). NaCl (ACS Reagent, Merck), NaOH (Titrisol®, Merck), HCl (Titrisol®, Merck), HClO_4 (Suprapur®, Merck), NaClO_4 (p.a., Merck), $\text{Ca}(\text{NO}_3)_2 \cdot 4\text{H}_2\text{O}$ (p.a., Merck) and Na_2CO_3 (p.a., Merck) were used without further purification. A crystalline calcium uranyl carbonate solid was synthesized following a modification of the method originally described by Meyrowitz et al. (1963). A 1.0 M U(VI) solution was prepared by dissolving 5.02 g of $\text{UO}_2(\text{NO}_3)_2 \cdot 6\text{H}_2\text{O}$ (p.a., Merck) in 10 mL of Milli-Q water. This solution was slowly added to 100 mL of a solution 0.3 M Na_2CO_3 . Then, 10 mL of 2.0 M $\text{Ca}(\text{NO}_3)_2$ were added dropwise under continuous agitation. Finally, the pH of the resulting solution was adjusted to pH 8.0 by slow titration with 0.1 M Na_2CO_3 , resulting in the fast formation of the targeted calcium uranyl carbonate solid. The fine crystalline, yellow-green solid was filtered (0.125 μm pore size) and washed 3 times with Milli-Q water. The wet solid was dried over 24 h under air. The dry weight of the resulting material yielded (72 ± 5) % of the theoretical value. The resulting solid phase was characterized by the multi-method approach described in Section 2.4.

2.2. pH measurement

A combination pH electrode (ROSS Orion or Mettler Toledo, with 3.0 M KCl as filling solution) calibrated against commercial pH buffers (pH = 7–11, Merck or HANNA Instruments) was used for the quantification of proton concentrations in molal units (as pH_m , with $\text{pH}_m = -\log [\text{H}^+]$). The calibration of the electrode was performed at $T = (22 \pm 3), (25 \pm 1)$ and $(80 \pm 5)^\circ\text{C}$. pH measurements at $T = 25$ and 80°C were performed with tempered vessels using a water circulating cooler (WOBSER GmbH, experiments at $T = 25^\circ\text{C}$) or a dry block heater system (IKA, experiments at $T = 80^\circ\text{C}$), respectively, coupled in both cases with a customized aluminum block. The values of pH_m were obtained from the measured pH values (pH_{exp}) and considering $\text{pH}_m = \text{pH}_{\text{exp}} + A_m$, where A_m is a correction factor entailing both the activity coefficient of H^+ and the liquid junction potential of the electrode for a given background electrolyte concentration and temperature. Empirical correction factors A_m for NaCl systems at $T = 22$ and 80°C were reported previously in Altmaier et al. (2003) and Endrizzi et al. (2018), respectively. A correction factor $A_m = -0.02$ was experimentally determined in this work for 0.1 m NaClO_4 solutions following the approach described in (Altmaier et al., 2003).

2.3. Solubility experiments

Two independent series of batch solubility samples were prepared in NaClO_4 and NaCl solutions in PTFE vials. In the first series, 5 g of the starting calcium uranyl carbonate solid (per sample) were equilibrated in 50 mL of 0.1 m NaClO_4 solutions at $T = (25 \pm 1)^\circ\text{C}$. In four independent samples, the pH_m was set to 7.0, 8.0, 8.3 and 9.0, and adjusted with 0.1 m HClO_4 or NaOH whenever necessary. Concentrations of U and Ca after ultrafiltration (25 nm pore size filters, Schleicher and Schuell) were monitored for up to 180 days by means of Inductively Coupled Plasma – Mass Spectrometry (ICP–MS, PerkinElmer Elan-5000) and Atomic Absorption Spectroscopy (AAS; PerkinElmer AAS 4100, with $\text{C}_2\text{H}_2\text{--N}_2\text{O}$ flame). After attaining equilibrium conditions, the total carbonate concentration in the aqueous phase of the investigated

samples was determined using an equipment Analytik Jena GmbH (IDC, 98704 Langenwiesen XII/95). A second series of solubility experiments was conducted by equilibrating ca. 250 mg of the starting calcium uranyl carbonate solid (per sample) in 5 mL of solution: (i) Milli-Q water, (ii) 0.51 m NaCl, and (iii) 5.61 m NaCl. Due to the pH titration with HCl and NaOH, sample (i) resulted in approximately ≈ 0.03 m NaCl. Each sample was prepared in duplicate and equilibrated at $T = 22$ and 80°C (six samples in total). The pH_m of the resulting samples was adjusted to 7.9–8.2 with the addition of HCl–NaCl and NaOH–NaCl solutions of the same ionic strength. This range of pH_m was chosen to minimize both $\text{CO}_2(\text{g})$ degassing and calcite precipitation in the experiments at room temperature, according with model calculations conducted using thermodynamic data summarized in Tables A-1 and A-2 of Appendix. A compact laboratory oven (Falc Instruments) was used for the batches equilibrating at $T = 80^\circ\text{C}$. Concentrations of uranium and pH_m were monitored for 132 days until attaining equilibrium conditions (defined as constant values of [U] and pH_m). Calcium concentrations were also measured after attaining equilibrium conditions. Total concentration of uranium and calcium were determined by ICP–MS (PerkinElmer ELAN 6100) and Inductively Coupled Plasma – Optical Emission Spectrometry (ICP–OES, PerkinElmer OPTIMA, 2000[™]), respectively, after phase separation and corresponding dilution with 2% HNO_3 . Phase separation was achieved by rapid syringe filtration (Pall Acrodisc[®] filters, pore size $0.1\ \mu\text{m}$, PTFE membrane), both for samples equilibrated at $T = 22$ and 80°C . This approach has been shown to minimize the temperature drop within the filtration process at elevated temperatures (Endrizzi et al., 2018). Values of concentration obtained in molar (M) units were converted to molal (m) units using the conversion factors reported in the NEA–TDB for different background electrolytes (Guillaumont et al., 2003).

2.4. Solid phase characterization

The starting calcium uranyl carbonate solid was characterized by XRD, quantitative chemical analysis, TG–DTA, IR and Raman spectroscopy. A fraction of the synthesized solid phase (ca. 100 mg) was characterized by XRD using a Universal-Röntgen-Diffraktometer (URD 6, Freiburger Präzisionsmechanik, Freiberg, Germany) (Cu $K\alpha$ radiation). Diffractograms were collected within $5^\circ \leq 2\theta \leq 60^\circ$, a step size of 0.05° and accumulation times of 60 s per single step. Diffraction patterns obtained in the present work were compared with reference patterns available in the JCPDS database (Joint Committee of Powder Diffraction Standards, JCPDS, 2001). An exact amount (2.01 g) of the calcium uranyl carbonate solid was dissolved in 0.1 M HNO_3 , and the concentrations of U and Ca measured by ICP–MS and AAS, respectively. TG–DTA measurements of the starting calcium uranyl carbonate solid (ca. 30 mg per sample) were performed with a Thermoanalyzer STA 92 (Setaram, France) using an aluminum crucible. The investigated temperature range covered 20–1100 $^\circ\text{C}$, with a temperature increase of $10^\circ\text{C}\cdot\text{min}^{-1}$. Measurements were conducted under an oxygen stream of $3\ \text{L}\cdot\text{h}^{-1}$. The buoyancy correction for the TGA was done by measuring a blank. The reference sample for DTA was Al_2O_3 . FT-IR spectra were recorded using a PerkinElmer GX–2000 instrument equipped with a Mercury Cadmium Telluride (MCT) detector. Spectral resolution was $4\ \text{cm}^{-1}$ in the frequency range from 4000 to $600\ \text{cm}^{-1}$. IR measurements were conducted with 50 mg of the starting material mixed with KBr and pressed as pellet. Diffuse-reflectance infrared Fourier transform (DRIFT) measurements were accomplished by mixing the crystalline compounds with solid KBr at approximately 0.2 wt%. Raman spectra were recorded using a Bruker RFS 100 FT-NIR Raman spectrometer (Bruker Analytik GmbH, Karlsruhe, Germany). The source of excitation for Raman spectroscopy was a 250 mW Nd:YAG laser system. The excitation wavelength was 1064 nm and the resolution of the system was $4\ \text{cm}^{-1}$. Spectra were recorded within 3500 and $100\ \text{cm}^{-1}$.

U(VI) solid phases were also characterized after finalizing the solubility experiments. A fraction of the samples equilibrated in NaClO_4

solutions (ca. 100 mg) was washed 5 times with Milli-Q water, and dried over 24 h under air atmosphere. The dried solid was characterized by XRD as described above for the starting calcium uranyl carbonate solid. Solid phases collected after completing the solubility experiments in NaCl systems at $T = 22$ and 80°C were characterized by XRD, quantitative chemical analysis and Scanning Electron Microscopy coupled with Energy-Dispersive X-ray Spectroscopy (SEM–EDS). Approximately 10 mg of each solid phase were separated and washed 3–5 times with 1 mL ethanol to remove any residuals from the background electrolyte. The largest fraction of the washed solid was characterized by XRD using a Bruker D8 Advance diffractometer (Cu $K\alpha$ radiation) equipped with a Sol-X detector. An air-tight sample holder with dome (Bruker) was used for the measurements. XRD data were collected within $5^\circ \leq 2\theta \leq 60^\circ$, a step size of 0.02° and accumulation times of 4–21 s per single step. The solid used for XRD measurements was dissolved in 2% HNO_3 , and the resulting solution used for the quantification of uranium (ICP–MS), calcium and sodium (ICP–OES). A small fraction of the washed solid (ca. 20 μg) was further characterized by SEM–EDS (Cambridge Instruments, CamScan CS 44 FE), which provided information on the morphology, particle size and elemental composition of the investigated uranium solid phases. Elemental composition determined by EDS was obtained as average of 6–9 spots in each solid phase.

2.5. Thermodynamic calculations

Thermodynamic data selected within the Thermochemical database project of the OECD Nuclear Energy Agency (NEA–TDB, (Guillaumont et al., 2003)) were considered to calculate the aqueous speciation of uranium in the presence of carbonate (binary uranium hydroxide and uranium carbonate species). Although not yet selected in the NEA–TDB (Guillaumont et al., 2003), the ternary aqueous species $\text{CaUO}_2(\text{CO}_3)_3^{2-}$ and $\text{Ca}_2\text{UO}_2(\text{CO}_3)_3(\text{aq})$ have been shown to play a relevant role in aqueous solutions containing calcium and carbonate under near neutral pH conditions (Bernhard et al., 1996; Dong and Brooks, 2006; Endrizzi and Rao, 2014; Lee and Yun, 2013; Prat et al., 2009). The possible formation of these ternary species in the conditions of our experiments was accordingly considered in the thermodynamic calculations using the corresponding equilibrium constants previously reported in the literature (Lee and Yun, 2013). The aqueous speciation of carbonate in the presence of calcium was calculated using thermodynamic data selected in the NEA–TDB (Guillaumont et al., 2003) and in ThermoChimie v.9b (Giffaut et al., 2014). Table A-1 in the Appendix summarizes all chemical reactions and corresponding equilibrium constants included in the thermodynamic calculations performed in this work.

The specific ion interaction theory (SIT) (Ciavatta, 1980; Grenthe et al., 2013) was used to account for ionic strength corrections in the equilibrium reactions involved in the thermodynamic calculations. In the SIT formalism, the activity coefficients of (charged) aqueous species (γ_i) are calculated as described in (1):

$$\log \gamma_i = -z_i^2 D + \sum \varepsilon_{ij} m_j \quad (1)$$

where z_i represents the charge of the given ionic species, D is the Debye–Hückel term ($D = (0.509\sqrt{I_m})/(1 + 1.5\sqrt{I_m})$ at 25°C), ε_{ij} is the specific ion-interaction coefficient for a pair of oppositely charged ions, m_j corresponds to the molal concentration of the ion j , and I_m is the ionic strength in molal units. Table A-2 in the Appendix summarizes all SIT ion interaction coefficients used in the thermodynamic calculations performed in the present work. The validity of SIT is normally delimited to $I_m \leq 3.5$ m, although a number of experimental studies have demonstrated the correct performance of the SIT approach to ionic strength conditions well beyond this limit (especially in 1:1 electrolytes like NaCl) (Altmaier et al., 2017; Gaona et al., 2013; Neck et al., 2009; Yalçıntaş et al., 2016).

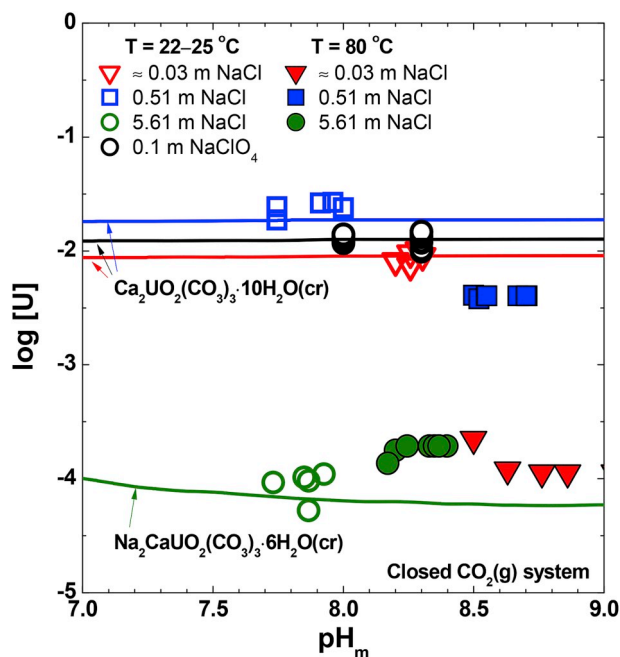


Fig. 1. Experimental solubility of $\text{Ca}_2\text{UO}_2(\text{CO}_3)_3 \cdot 10\text{H}_2\text{O}(\text{cr})$ equilibrated in $\approx 0.03\text{ m NaCl}$, 0.51 and 5.61 m NaCl solutions ($T = 22$ and 80°C), as well as in 0.1 m NaClO_4 ($T = 25^\circ\text{C}$). Solid lines represent the calculated solubility at room temperature using $\log K_{s,0}^{\circ}\{\text{Ca}_2\text{UO}_2(\text{CO}_3)_3 \cdot 10\text{H}_2\text{O}(\text{cr})\}$ ($\approx 0.03\text{ m NaCl}$, 0.1 m NaClO_4 and 0.51 m NaCl systems) and $\log K_{s,0}^{\circ}\{\text{Na}_2\text{CaUO}_2(\text{CO}_3)_3 \cdot 6\text{H}_2\text{O}(\text{cr})\}$ (5.61 m NaCl system) determined in this work, in combination with thermodynamic and activity models summarized in Section 2.4 for aqueous species. Thermodynamic calculations performed assuming closed $\text{CO}_2(\text{g})$ systems and excluding calcite precipitation.

3. Results

3.1. Solubility data at $T = 22-80^\circ\text{C}$

Fig. 1 shows the experimental solubility data of U(VI) (as $\log [\text{U}]$ vs. pH_m) determined in NaClO_4 ($T = 25^\circ\text{C}$) and NaCl ($T = 22$ and 80°C) systems. Table 1 and Table 2 summarize additional information on the pH_m (initial and final for NaCl systems), $[\text{U}]$, $[\text{Ca}]$, $\text{Ca} : \text{U}$ ratio and C_{tot} (total inorganic carbon, in m) in the aqueous phase after attaining equilibrium conditions. Rather high concentrations of uranium ($\approx 10^{-2}\text{ m}$) are measured at room temperature for the calcium uranyl carbonate phase equilibrated in $\approx 0.03\text{ m NaCl}$, 0.1 m NaClO_4 and 0.51 m NaCl systems (Fig. 1). A significant drop in solubility is observed for the system in 5.61 m NaCl equilibrated at $T = 22^\circ\text{C}$, as well as for all systems equilibrated at $T = 80^\circ\text{C}$. The drop in solubility at elevated temperature is accompanied by a clear change in the visual color of the solid phase, from yellow to orange. Both observations strongly hint towards a solid phase transformation. A remarkable shift in pH_m towards more alkaline conditions is also observed in the solubility samples equilibrated at $T = 80^\circ\text{C}$ ($0.5-0.8\text{ pH}_m$ -units, see Table 1). According to Henry's law, the dissolution of $\text{CO}_2(\text{g})$ in water is less favored at elevated temperatures (Gordon and Jones, 1973). This promotes the degassing of $\text{CO}_2(\text{g})$ from the aqueous solution and the consequent increase of pH_m observed in our experiments at elevated temperature. On the contrary, no significant changes in pH_m are observed in the solubility experiments at $T = 22^\circ\text{C}$, thus supporting that $\text{CO}_2(\text{g})$ equilibrium is maintained in this range of pH_m and $[\text{Ca}]$, as predicted by the thermodynamic calculations described in Section 2.4.

Remarkably high aqueous concentrations of uranium and calcium are measured for the calcium uranyl phase equilibrated at room temperature in 0.1 m NaClO_4 (samples A–D), $\approx 0.03\text{ m NaCl}$ (sample E) and 0.51 m NaCl (sample F), in all cases showing a ratio $\text{Ca} : \text{U} \approx 2 : 1$. This

observation indicates: (i) a congruent dissolution of the calcium uranyl phase, expectedly $\text{Ca}_2\text{UO}_2(\text{CO}_3)_3 \cdot 10\text{H}_2\text{O}(\text{cr})$, and (ii) no precipitation of other phases containing Ca, e.g. calcite. Sample G (equilibrated in 5.61 m NaCl at $T = 22^\circ\text{C}$) shows a significant decrease in uranium concentration, whilst retaining a rather high concentration of calcium in solution. These observations strongly hint towards the formation of a new solid phase with significantly lower solubility (within these boundary conditions) and with a ratio $\text{Ca} : \text{U} < 2$.

A significant drop in the concentrations of uranium and calcium is observed for samples H ($\approx 0.03\text{ m NaCl}$, $T = 80^\circ\text{C}$) and I (0.51 m NaCl , $T = 80^\circ\text{C}$), compared to the analogous samples investigated at $T = 22^\circ\text{C}$. Somehow similar uranium concentrations are measured for 5.61 m NaCl systems at $T = 22$ and 80°C , whereas a significantly lower concentration of calcium is measured in the latter system (Table 1). Besides the likely transformation of the original uranium solid phase, these observations hint towards the precipitation of calcite in the system equilibrated at elevated temperature. This hypothesis is also in line with the increase in pH_m observed in the solubility samples equilibrated at elevated temperature.

Experimental measurements of the total carbonate concentration (C_{tot}) in solution after attaining equilibrium conditions in samples A–D are in good agreement with calculated C_{tot} assuming a congruent dissolution of the calcium uranyl phase ($C_{\text{tot}} = 3 \times [\text{U}]_{\text{tot}} = 3/2 \times [\text{Ca}]_{\text{tot}}$), expectedly $\text{Ca}_2\text{UO}_2(\text{CO}_3)_3 \cdot 10\text{H}_2\text{O}(\text{cr})$. Experimentally measured C_{tot} in samples B–D ($\text{pH}_m = 8-9$) also agree with carbonate concentration calculated assuming equilibrium with air (with $\log P_{\text{CO}_2} = -3.5$). On the contrary, C_{tot} measured in sample A ($\text{pH}_m = 7$) is significantly larger than the total carbonate concentration calculated for this pH_m assuming equilibrium with air. These results support that equimolar dissolution of carbonate should be expected also for samples E–G, for which the calcium uranyl carbonate solid was equilibrated in NaCl solutions with $\text{pH}_m = 7.8-8.3$ at $T = 22^\circ\text{C}$.

3.2. Solid phase characterization

XRD patterns of the starting calcium uranyl carbonate solid shown in Fig. 2a are in excellent agreement with reference patterns reported in the JCPDS database for liebigite, $\text{Ca}_2\text{UO}_2(\text{CO}_3)_3 \cdot 10\text{H}_2\text{O}(\text{cr})$ (JCPDS file number 49-1056). Quantitative chemical analysis of this solid resulted in $(33.9 \pm 0.6)\text{ wt}\%$ U and $(11.5 \pm 0.5)\text{ wt}\%$ Ca, consistent with the theoretical values $33.5\text{ wt}\%$ and $11.3\text{ wt}\%$ calculated for $\text{Ca}_2\text{UO}_2(\text{CO}_3)_3 \cdot 10\text{H}_2\text{O}(\text{cr})$. TG and DTA data obtained for the starting calcium uranyl carbonate solid are summarized in Figure A-1 and Table A-3 in the Appendix. The quantitative evaluation of these data indicates a content of $(10.1 \pm 0.3)\text{ mol}$ of H_2O and $(3.4 \pm 0.3)\text{ mol}$ of CO_2 in the starting solid. The IR spectrum of the calcium uranyl carbonate solid is shown in Figure A-2 of the Appendix, together with the IR spectra of the reagents used in the synthesis ($\text{UO}_2(\text{NO}_3)_2 \cdot 6\text{H}_2\text{O}$, $\text{Ca}(\text{NO}_3)_2 \cdot 4\text{H}_2\text{O}$ and Na_2CO_3). The IR spectrum collected in this work agrees well with previous IR data reported for liebigite (Cejka and Urbanec, 1999; Chemorukov et al., 2009; Urbanec and Cejka, 1979), and provides additional evidence on the absence of impurities in the synthesized calcium uranyl carbonate solid. Raman data collected for the calcium uranyl carbonate solid investigated in this work are shown in Figure A-3 of the Appendix. The thorough solid phase characterization described above confirms the stoichiometry of the starting solid phase used in this solubility study as $\text{Ca}_2\text{UO}_2(\text{CO}_3)_3 \cdot 10\text{H}_2\text{O}(\text{cr})$.

Solid phases equilibrated in NaClO_4 solutions were characterized by XRD after finalizing the solubility experiments. XRD patterns shown in Fig. 2a for samples A–D are consistent with those collected for the starting $\text{Ca}_2\text{UO}_2(\text{CO}_3)_3 \cdot 10\text{H}_2\text{O}(\text{cr})$ solid, thus confirming that no solid phase transformation occurred in the course of the solubility experiment.

XRD patterns of solid phases recovered from solubility experiments in NaCl solutions at $T = 22^\circ\text{C}$ (samples E–G) and 80°C (samples H–J) are shown in Fig. 2b–c, respectively. Table 3 summarizes the ratio $\text{Ca} : \text{U}$ and $\text{Na} : \text{U}$ determined for the same solid phases by SEM–EDS and quantitative

Table 1

Summary of pH_m (initial and final in NaCl systems, see text), and aqueous concentrations of uranium and calcium after attaining equilibrium conditions. Relative standard error in measured uranium and calcium concentrations are typically $< 10\%$, or $< 20\%$ in 5.61 m NaCl. Uncertainty in pH_m measurements is ± 0.05 .

Sample	T ($^{\circ}\text{C}$)	pH_m^a	$[\text{NaClO}_4]$ (m)	$[\text{U}]$ ($\times 10^{-3}$ m)	$[\text{Ca}]$ ($\times 10^{-3}$ m)	Ca : U ratio	
A	(25 \pm 1)	7.0	0.1	11.9	23.9	2.0	
B		8.0	0.1	13.9	27.5	2.0	
C		8.3	0.1	14.7	29.5	2.0	
D		9.0	0.1	15.8	31.6	2.0	
Sample	T ($^{\circ}\text{C}$)	Initial pH_m	Final pH_m	$[\text{NaCl}]$ (m)	$[\text{U}]$ ($\times 10^{-3}$ m)	$[\text{Ca}]$ ($\times 10^{-3}$ m)	Ca : U ratio
E	(22 \pm 3)	8.1	8.3	$\approx 0.03^b$	8.5	17.9	2.1
F		8.1	7.8	0.51	21.6	40.0	1.9
G		8.1	7.9	5.61	0.08	65.4	785
Sample	T ($^{\circ}\text{C}$)	pH_m	$[\text{NaCl}]$ (m)	$[\text{U}]$ ($\times 10^{-3}$ m)	$[\text{Ca}]$ ($\times 10^{-3}$ m)	Ca : U ratio	
H	(80 \pm 5)	8.2	9.0	$\approx 0.03^b$	0.05	n.d.	n.d.
I		8.2	8.7	0.51	3.6	n.d.	n.d.
J		7.9	8.4	5.61	0.15	0.18	1.2

^a Kept constant throughout the solubility experiment with $\text{HClO}_4/\text{NaOH}$ titrations; ^b Resulting from the pH_m adjustments; Milli-Q as original solution.

Table 2

Total carbonate concentration (C_{tot}) measured in the aqueous solution of the solubility samples A–D after attaining equilibrium conditions and calculated using two different approximations.

Sample	pH_m	C_{tot} (m) ($\times 10^{-3}$)		
		Experimental	Calculated I ^a	Calculated II ^b
A	7.0	(33.8 \pm 3.3)	35.7	15.8
B	8.0	(45.0 \pm 4.3)	41.7	38.6
C	8.3	(45.5 \pm 5.0)	44.1	40.2
D	9.0	(51.9 \pm 7.0)	47.4	54.8

^a Calculated assuming congruent dissolution of $\text{Ca}_2\text{UO}_2(\text{CO}_3)_3 \cdot 10\text{H}_2\text{O}(\text{cr})$, $C_{\text{tot}} = 3 \times [\text{U}]_{\text{exp}}$.

^b Calculated assuming equilibrium of carbonate with atmospheric CO_2 ($\log P_{\text{CO}_2} = -3.5$).

chemical analysis. XRD patterns collected for samples E and F match with those available for the reference $\text{Ca}_2\text{UO}_2(\text{CO}_3)_3 \cdot 10\text{H}_2\text{O}(\text{cr})$ (JCPDS file number 49–1056) very well. The significantly poorer signal-to-noise ratio in the XRD of these samples, compared to that of the starting material and samples A–D is potentially caused by a combination of several factors, e.g.

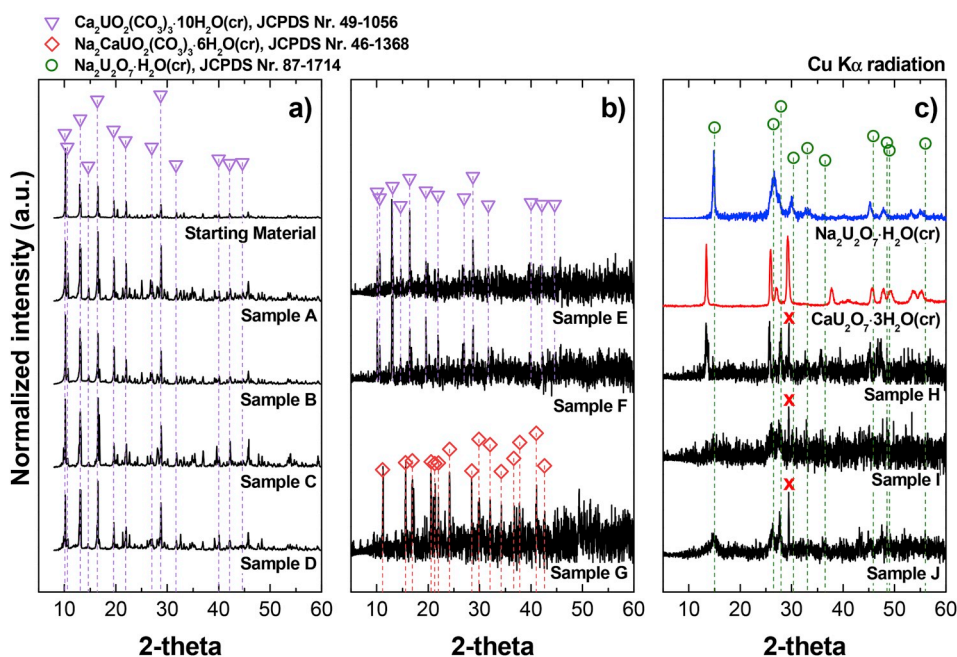


Fig. 2. Powder X-ray diffraction patterns of solid U(VI) phases: (a) starting material, $\text{Ca}_2\text{UO}_2(\text{CO}_3)_3 \cdot 10\text{H}_2\text{O}(\text{cr})$, and solid phases after terminating solubility experiments in 0.1 m NaClO_4 at $T = 25^{\circ}\text{C}$; (b) solid phases after terminating solubility experiments at $T = 22^{\circ}\text{C}$; (c) solid phases after terminating solubility experiments at $T = 80^{\circ}\text{C}$. Symbols corresponding to reference patterns reported in the JCPDS database for $\text{Ca}_2\text{UO}_2(\text{CO}_3)_3 \cdot 10\text{H}_2\text{O}(\text{cr})$, $\text{Na}_2\text{CaUO}_2(\text{CO}_3)_3 \cdot 6\text{H}_2\text{O}(\text{cr})$ and $\text{Na}_2\text{U}_2\text{O}_7 \cdot \text{H}_2\text{O}(\text{cr})$. XRD patterns reported by Altmaier and co-workers (Altmaier et al., 2005, 2017) for $\text{CaU}_2\text{O}_7 \cdot 3\text{H}_2\text{O}(\text{cr})$ and $\text{Na}_2\text{U}_2\text{O}_7 \cdot \text{H}_2\text{O}(\text{cr})$, respectively, are appended for comparison. Red crosses in figure (c) mark the main reflection of calcite (104). (For interpretation of the references to color in this figure legend, the reader is referred to the Web version of this article.)

Table 3

Ca : U and Na : U ratios in the solid phases after solubility experiments (NaCl systems, $T = 22$ and 80°C) as quantified by SEM–EDS and quantitative chemical analysis (U: ICP–MS/OES; Ca: ICP–OES). Relative standard errors for ratios quantified by SEM–EDS are $< 10\%$, except for samples at $T = 80^{\circ}\text{C}$ (relative standard errors $< 20\%$) due to the heterogeneous distribution of calcite precipitates. Relative standard errors for atomic ratios quantified by ICP–MS/OES are $< 10\%$ (dilute systems) or $< 20\%$ (5.61 m NaCl).

Sample	SEM–EDS		ICP–MS/OES	
	Ca : U	Na : U	Ca : U	Na : U
E, ≈ 0.03 m NaCl ($T = 22^{\circ}\text{C}$)	2.3	–	2.1	–
F, 0.51 m NaCl ($T = 22^{\circ}\text{C}$)	1.8	–	2.0	–
G, 5.61 m NaCl ($T = 22^{\circ}\text{C}$)	1.0	2.0	1.1	1.9
H, ≈ 0.03 m NaCl ($T = 80^{\circ}\text{C}$)	0.5	0.4	2.3	0.2
I, 0.51 m NaCl ($T = 80^{\circ}\text{C}$)	0.6	1.2	2.3	0.9
J, 5.61 m NaCl ($T = 80^{\circ}\text{C}$)	0.2	1.6	2.3	1.7

equipment configuration, accumulation time and amount of sample material used for XRD acquisition. XRD patterns of the U(VI) solid phase equilibrated in 5.61 m NaCl at $T = 22^{\circ}\text{C}$ (sample G) are strikingly different, and show a good agreement with reference patterns reported for

andersonite, $\text{Na}_2\text{CaUO}_2(\text{CO}_3)_3 \cdot 6\text{H}_2\text{O}(\text{cr})$ (JCPDS file number 46-1368). These data are also in agreement with the comprehensive characterization of a synthetic andersonite previously conducted by Amayri and co-workers (Amayri et al., 2004). The predominance of two different solid phases at $T = 22^\circ\text{C}$ (depending upon background electrolyte concentration) is in line with solubility data discussed in Section 3.1.

A clear transformation of the original $\text{Ca}_2\text{UO}_2(\text{CO}_3)_3 \cdot 10\text{H}_2\text{O}(\text{cr})$ is observed in the diffractograms of all solubility samples equilibrated at $T = 80^\circ\text{C}$ (Fig. 2c). XRD patterns support the formation of $\text{Na}_2\text{U}_2\text{O}_7 \cdot \text{H}_2\text{O}(\text{cr})$ in the solubility samples equilibrated at elevated temperature in 0.51 m and 5.61 m of NaCl solutions (samples I and J). Well-defined and clearly changed XRD patterns are observed for sample H (≈ 0.03 m NaCl, $T = 80^\circ\text{C}$), compared to samples I and J. Hence, the first and most prominent peak in the XRD of sample H is significantly shifted towards lower 2θ values, compared to reference patterns of $\text{Na}_2\text{U}_2\text{O}_7 \cdot \text{H}_2\text{O}(\text{cr})$ ($2\theta = 13.4^\circ$ vs. $2\theta = 14.9\text{--}15.0^\circ$). Indeed, XRD patterns of sample H show close similarities with patterns reported by Altmaier and co-workers for $\text{CaU}_2\text{O}_7 \cdot 3\text{H}_2\text{O}(\text{cr})$ (Altmaier et al., 2005) (see Fig. 2c). The latter phase was reported to control the solubility of U(VI) in alkaline, dilute to concentrated CaCl_2 solutions (in the absence of carbonate) (Altmaier et al., 2005). We note further that XRD patterns collected for sample H disregard the presence of becquerelite, $\text{CaU}_6\text{O}_{19} \cdot 11\text{H}_2\text{O}(\text{cr})$.

Sharp XRD peaks located at $2\theta \approx 29.4^\circ$ are systematically observed for all solid phases equilibrated at elevated temperatures, whereas such a feature is missing in the diffractograms of solid phases equilibrated at room temperature. This peak can be assigned to the main reflection of calcite (104), thus indicating the formation of this solid phase only in the samples equilibrated at $T = 80^\circ\text{C}$. These observations agree with calcium concentrations in the aqueous phase measured in the solubility experiments at $T = 22$ and 80°C .

Ratios Ca : U and Na : U determined by SEM-EDS and quantitative chemical analysis are in excellent agreement with XRD data and support the predominance of $\text{Ca}_2\text{UO}_2(\text{CO}_3)_3 \cdot 10\text{H}_2\text{O}(\text{cr})$ (samples E and F) and $\text{Na}_2\text{CaUO}_2(\text{CO}_3)_3 \cdot 6\text{H}_2\text{O}(\text{cr})$ (sample G) at room temperature. A more complex picture arises in the SEM-EDS and quantitative chemical analysis of samples equilibrated at $T = 80^\circ\text{C}$. For these systems, significantly higher Ca : U ratios are measured by quantitative chemical analyses than by SEM-EDS. The first method provides an average Ca : U ratio of all solid phases present in the system, whereas SEM-EDS gives insight mostly (although not exclusively) on the composition of the uranium phases targeted during analysis. Hence, the ratio Ca : U ≈ 2 measured for these samples by quantitative chemical analysis reflect that the inventories of U and Ca are mostly found as solid phases, expectedly in the form of uranium compounds and calcite. A ratio Na : U ≈ 1.5 is measured for sample J, both by SEM-EDS and quantitative chemical analysis. In combination with XRD data, these results provide additional support on the formation of $\text{Na}_2\text{U}_2\text{O}_7 \cdot \text{H}_2\text{O}(\text{cr})$ in 5.61 m NaCl solutions equilibrated at $T = 80^\circ\text{C}$. SEM-EDS of samples H and I suggest the co-existence of Na and Ca in the U(VI) solid phases forming at elevated temperature. In combination with XRD data, these results strongly support that the original $\text{Ca}_2\text{UO}_2(\text{CO}_3)_3 \cdot 10\text{H}_2\text{O}(\text{cr})$ transformed to Na- and Ca-uranates at $T = 80^\circ\text{C}$.

Fig. 3 shows the SEM images of all solid phases investigated in the present work. The original U(VI) material (Fig. 3a), sample E (Fig. 3b) and sample F (Fig. 3c) show a similar morphology and particle size, in good agreement by the confirmed predominance of $\text{Ca}_2\text{UO}_2(\text{CO}_3)_3 \cdot 10\text{H}_2\text{O}(\text{cr})$. The morphology of sample G (Fig. 3d) shows a distinctive crystalline structure, in line with the transformation of $\text{Ca}_2\text{UO}_2(\text{CO}_3)_3 \cdot 10\text{H}_2\text{O}(\text{cr})$ into $\text{Na}_2\text{CaUO}_2(\text{CO}_3)_3 \cdot 6\text{H}_2\text{O}(\text{cr})$ indicated by XRD. All samples equilibrated at $T = 80^\circ\text{C}$ show smaller particle size and a less crystalline character (Fig. 3e–g), compared to the morphology of the original U(VI) material shown in Fig. 3a. These observations are also in line with XRD data supporting the transformation of $\text{Ca}_2\text{UO}_2(\text{CO}_3)_3 \cdot 10\text{H}_2\text{O}(\text{cr})$ into less crystalline Na- and Ca-uranates at elevated temperatures.

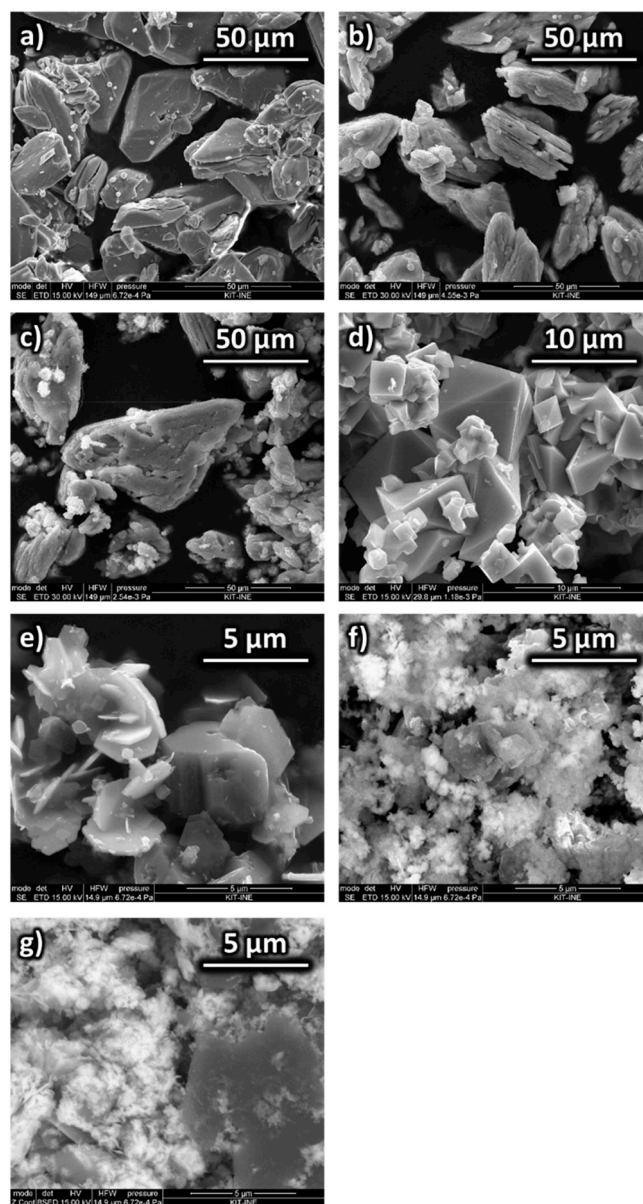


Fig. 3. SEM images of (a) initial U(VI) material, $\text{Ca}_2\text{UO}_2(\text{CO}_3)_3 \cdot 10\text{H}_2\text{O}(\text{cr})$; solid phases equilibrated at $T = 22^\circ\text{C}$: (b) in ≈ 0.03 m NaCl, (c) 0.51 m NaCl, (d) 5.61 m NaCl; solid phases equilibrated at $T = 80^\circ\text{C}$: (e) in ≈ 0.03 m NaCl, (f) 0.51 m NaCl, (g) 5.61 m NaCl.

4. Discussion

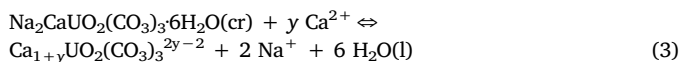
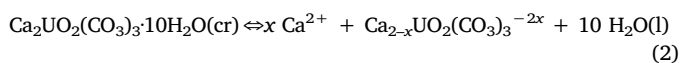
4.1. Thermodynamic model for the system

$\text{UO}_2^{2+} - \text{Ca}^{2+} - \text{Na}^+ - \text{H}^+ - \text{CO}_2(\text{g}) - \text{HCO}_3^- - \text{CO}_3^{2-} - \text{H}_2\text{O}(\text{l})$ at room temperature

Solid phases controlling the solubility of U(VI) in the investigated background electrolyte solutions at room temperature are identified as $\text{Ca}_2\text{UO}_2(\text{CO}_3)_3 \cdot 10\text{H}_2\text{O}(\text{cr})$ (in ≈ 0.03 m NaCl, 0.1 m NaClO_4 and 0.51 m NaCl solutions) and $\text{Na}_2\text{CaUO}_2(\text{CO}_3)_3 \cdot 6\text{H}_2\text{O}(\text{cr})$ (in 5.61 m NaCl solutions). Accordingly, experimental solubility data obtained in these conditions in combination with thermodynamic data available for the aqueous speciation of U(VI) in the presence of carbonate and calcium (see Section 2.4, and Tables A1 and A2 in the Appendix) are used to derive the values of $\log K_{s,0}^{\{\text{Ca}_2\text{UO}_2(\text{CO}_3)_3 \cdot 10\text{H}_2\text{O}(\text{cr})\}}$ and $\log K_{s,0}^{\{\text{Na}_2\text{CaUO}_2(\text{CO}_3)_3 \cdot 6\text{H}_2\text{O}(\text{cr})\}}$ at infinite dilution. Solubility data collected in 0.1 m NaClO_4 at $\text{pH}_m = 7$ and 9 have been disregarded

in this thermodynamic evaluation because of the large oversaturation with respect to $\text{CO}_2(\text{g})$ in air and to calcite, respectively. Indeed, solubility samples at $\text{pH}_m \approx 8\text{--}8.3$ are also slightly oversaturated with respect to calcite (saturation index, $\text{SI} < 0.4$, see Table A-4 in the Appendix), although calcite was not observed (by XRD) in any of these samples. This fact in itself does not affect the calculated thermodynamic data, provided that reliable solid phase characterization and accurate quantification of $[\text{U}]_{\text{tot}}$, $[\text{Ca}]_{\text{tot}}$ and C_{tot} are available. Furthermore, the calculation of the SI of calcite in the investigated system is strongly affected by the binary $\text{U}(\text{VI})\text{--CO}_3$ and ternary $\text{Ca}\text{--U}(\text{VI})\text{--CO}_3$ complexes forming in the aqueous phase. We draw the attention to the relevant impact of the species $(\text{UO}_2)_2\text{CO}_3(\text{OH})_3^-$ in the calculated SI of calcite, and the possible overestimation of its stability with the thermodynamic data currently selected in the NEA-TDB (Guillaumont et al., 2003). Solubility data obtained at $T = 80^\circ\text{C}$ are disregarded for the determination of any thermodynamic function because of the ill-defined solid phases controlling the solubility of $\text{U}(\text{VI})$ and the unknown carbonate concentration in aqueous solution after the partial loss of $\text{CO}_2(\text{g})$ observed in all samples equilibrated at this temperature.

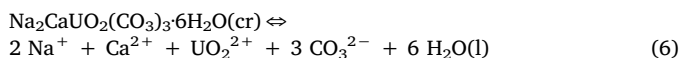
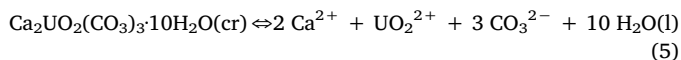
At room temperature, the solubility of $\text{Ca}_2\text{UO}_2(\text{CO}_3)_3 \cdot 10\text{H}_2\text{O}(\text{cr})$ and $\text{Na}_2\text{CaUO}_2(\text{CO}_3)_3 \cdot 6\text{H}_2\text{O}(\text{cr})$ within the investigated boundary conditions is mostly controlled by the equilibrium reactions (2) and (3), respectively:



with $0 \leq x \leq 2$ and $-1 \leq y \leq 1$. The use of thermodynamic data summarized in Table A-1 of the Appendix allows to calculate $[\text{UO}_2^{2+}]_{\text{free}}$, $[\text{Ca}^{2+}]_{\text{free}}$ and $[\text{CO}_3^{2-}]_{\text{free}}$ from the values of pH_m , $[\text{U}]_{\text{tot}}$, $[\text{Ca}]_{\text{tot}}$ and C_{tot} described in eq. (4),

$$C_{\text{tot}} = [\text{H}_2\text{CO}_3^*] + [\text{HCO}_3^-] + [\text{CO}_3^{2-}] + [\text{CaHCO}_3^+] + \sum c [\text{Ca}_a(\text{UO}_2)_b(\text{CO}_3)_c]^{2a+2b-2c} \quad (4)$$

with $0 \leq a \leq 2$, $0 \leq b \leq 3$, and $0 \leq c \leq 6$. Reactions (2) and (3) can be then redefined in the form of solubility reactions (5) and (6), resulting in the corresponding solubility products at $I \neq 0$, eq. (7) – (8), and at infinite dilution, eq. (9) – (10):



with

$$\log K'_{s,0}\{\text{Ca}_2\text{UO}_2(\text{CO}_3)_3 \cdot 10\text{H}_2\text{O}(\text{cr})\} = 2 \log [\text{Ca}^{2+}]_{\text{free}} + \log [\text{UO}_2^{2+}]_{\text{free}} + 3 \log [\text{CO}_3^{2-}]_{\text{free}} \quad (7)$$

$$\log K'_{s,0}\{\text{Na}_2\text{CaUO}_2(\text{CO}_3)_3 \cdot 6\text{H}_2\text{O}(\text{cr})\} = 2 \log [\text{Na}^+] + \log [\text{Ca}^{2+}]_{\text{free}} + \log [\text{UO}_2^{2+}]_{\text{free}} + 3 \log [\text{CO}_3^{2-}]_{\text{free}} \quad (8)$$

and

$$\log K^{\circ}_{s,0}\{\text{Ca}_2\text{UO}_2(\text{CO}_3)_3 \cdot 10\text{H}_2\text{O}(\text{cr})\} = \log K'_{s,0}\{\text{Ca}_2\text{UO}_2(\text{CO}_3)_3 \cdot 10\text{H}_2\text{O}(\text{cr})\} + 2 \log \gamma\{\text{Ca}^{2+}\} + \log \gamma\{\text{UO}_2^{2+}\} + 3 \log \gamma\{\text{CO}_3^{2-}\} + 10 \log a_w \quad (9)$$

$$\log K^{\circ}_{s,0}\{\text{Na}_2\text{CaUO}_2(\text{CO}_3)_3 \cdot 6\text{H}_2\text{O}(\text{cr})\} = \log K'_{s,0}\{\text{Na}_2\text{CaUO}_2(\text{CO}_3)_3 \cdot 6\text{H}_2\text{O}(\text{cr})\} + 2 \log \gamma\{\text{Na}^+\} + \log \gamma\{\text{Ca}^{2+}\} + \log \gamma\{\text{UO}_2^{2+}\} + 3 \log \gamma\{\text{CO}_3^{2-}\} + 6 \log a_w \quad (10)$$

Activity coefficients required for the determination of $\log K^{\circ}_{s,0}\{\text{Ca}_2\text{UO}_2(\text{CO}_3)_3 \cdot 10\text{H}_2\text{O}(\text{cr})\}$ and $\log K^{\circ}_{s,0}\{\text{Na}_2\text{CaUO}_2(\text{CO}_3)_3 \cdot 6\text{H}_2\text{O}(\text{cr})\}$ are calculated using the SIT formalism described in Section 2.4 and the SIT interaction coefficients summarized in Table A-2. The activity of water in 0.5 and 5.0 M NaCl was taken as reported in the NEA-TDB tables (Guillaumont et al., 2003). The values of pH_m , $[\text{U}]_{\text{tot}}$, $[\text{Ca}]_{\text{tot}}$ and C_{tot} were

determined experimentally in NaClO_4 systems. In $\approx 0.03 \text{ m}$ and 0.51 m NaCl systems, total carbonate concentrations are calculated as $C_{\text{tot}} = 3 \times [\text{U}]_{\text{tot}}$, which assumes a congruent dissolution of the starting $\text{Ca}_2\text{UO}_2(\text{CO}_3)_3 \cdot 10\text{H}_2\text{O}(\text{cr})$ solid. In 5.61 m NaCl and due to the formation of the secondary phase $\text{Na}_2\text{CaUO}_2(\text{CO}_3)_3 \cdot 6\text{H}_2\text{O}(\text{cr})$ with lower solubility, total carbonate concentration was calculated from the mass-balance with the known $[\text{U}]_{\text{tot}}$ and $[\text{Ca}]_{\text{tot}}$.

The contribution of charged uranium, calcium and carbonate species to the overall ionic strength was calculated using an iterative process with the software MATLAB. This contribution is mostly relevant for the system equilibrated in $\approx 0.03 \text{ m}$ NaCl. Conditional solubility products of $\text{Ca}_2\text{UO}_2(\text{CO}_3)_3 \cdot 10\text{H}_2\text{O}(\text{cr})$ and $\text{Na}_2\text{CaUO}_2(\text{CO}_3)_3 \cdot 6\text{H}_2\text{O}(\text{cr})$ determined at each ionic strength and corresponding extrapolation to $I = 0$ using SIT are summarized in Table 4. We note that similar results of $\log K^{\circ}_{s,0}\{\text{Ca}_2\text{UO}_2(\text{CO}_3)_3 \cdot 10\text{H}_2\text{O}(\text{cr})\}$ and $\log K^{\circ}_{s,0}\{\text{Na}_2\text{CaUO}_2(\text{CO}_3)_3 \cdot 6\text{H}_2\text{O}(\text{cr})\}$ were obtained assuming open systems (with $\text{pCO}_2(\text{g}) = 10^{-3.5} \text{ atm}$) to calculate C_{tot} . The excellent agreement in $\log K^{\circ}_{s,0}\{\text{Ca}_2\text{UO}_2(\text{CO}_3)_3 \cdot 10\text{H}_2\text{O}(\text{cr})\}$ determined in three independent solubility datasets in $\approx 0.03 \text{ m}$ NaCl, 0.1 m NaClO_4 (at two different pH_m) and 0.51 m NaCl provides additional confidence in the proposed chemical and thermodynamic models. The value of $\log K^{\circ}_{s,0}\{\text{Na}_2\text{CaUO}_2(\text{CO}_3)_3 \cdot 6\text{H}_2\text{O}(\text{cr})\}$ in Table 3 is provided with an increased uncertainty (± 0.5 instead of ± 0.2) to account for the fact that only experimental data in 5.61 m NaCl are available and that $\varepsilon(\text{CaUO}_2(\text{CO}_3)_3^{2-}, \text{Na}^+)$ (predominant aqueous species in these conditions, together with $\text{UO}_2(\text{CO}_3)_3^{4-}$) is an estimated value obtained by analogy with $\varepsilon(\text{UO}_2(\text{CO}_3)_2^{2-}, \text{Na}^+) = -(0.02 \pm 0.09) \text{ kg}\cdot\text{mol}^{-1}$ as reported in the NEA-TDB (Guillaumont et al., 2003).

Solubility products determined in this work for $\text{Ca}_2\text{UO}_2(\text{CO}_3)_3 \cdot 10\text{H}_2\text{O}(\text{cr})$ and $\text{Na}_2\text{CaUO}_2(\text{CO}_3)_3 \cdot 6\text{H}_2\text{O}(\text{cr})$ are used in combination with thermodynamic data available for the aqueous speciation of $\text{U}(\text{VI})$ to calculate the solubility of $\text{U}(\text{VI})$ at room temperature under the investigated experimental conditions (see Fig. 1) and assuming closed $\text{CO}_2(\text{g})$ systems. The figure shows an excellent agreement between experimental and calculated solubility for the different background electrolytes and background electrolyte concentrations.

Alwan and Williams reported the solubility products, $\Delta_r G^\circ$ and $\Delta_r H^\circ$ of $\text{Ca}_2\text{UO}_2(\text{CO}_3)_3 \cdot 10\text{H}_2\text{O}(\text{cr})$, $\text{Na}_2\text{CaUO}_2(\text{CO}_3)_3 \cdot 6\text{H}_2\text{O}(\text{cr})$, $\text{Mg}_2\text{UO}_2(\text{CO}_3)_3 \cdot 18\text{H}_2\text{O}(\text{cr})$ and $\text{CaMgUO}_2(\text{CO}_3)_3 \cdot 12\text{H}_2\text{O}(\text{cr})$ based on their solubility experiments at $T = 274\text{--}294 \text{ K}$ under a CO_2 -free atmosphere (Alwan and Williams, 1980). Aqueous concentrations of uranium in equilibrium with these solid phases were measured after one week, whereas stoichiometric (congruent) dissolution was assumed to calculate the concentrations of sodium, calcium and magnesium. As discussed by Endrizzi and co-workers (Endrizzi et al., 2016), the calculation of the solubility products in (Alwan and Williams, 1980) assumed the predominance of binary $\text{U}(\text{VI})\text{--carbonate}$ species in the aqueous phase. The solubility products reported in (Alwan and Williams, 1980) are recalculated in the present work considering also the formation of the ternary species $\text{CaUO}_2(\text{CO}_3)_3^{2-}$ and $\text{Ca}_2\text{UO}_2(\text{CO}_3)_3(\text{aq})$ in the aqueous phase. No experimental solubility data were provided by Alwan and Williams, and thus total aqueous concentrations of sodium, calcium, uranium, and carbonate are calculated in the present work from the reported solubility products and considering the stability constants used in (Alwan and Williams, 1980) for the calculation of the aqueous speciation (see Table A-1 in the Appendix). The resulting solubility products, $\log K^{\circ}_{s,0}\{\text{Ca}_2\text{UO}_2(\text{CO}_3)_3 \cdot 10\text{H}_2\text{O}(\text{cr})\} = -(32.1 \pm 1.0)$ and $\log K^{\circ}_{s,0}\{\text{Na}_2\text{CaUO}_2(\text{CO}_3)_3 \cdot 6\text{H}_2\text{O}(\text{cr})\} = -(31.9 \pm 2.9)$, agree well with the solubility products determined in the present work (see Table 4).

We note that thermodynamic data reported in Table 4 for $\text{Ca}_2\text{UO}_2(\text{CO}_3)_3 \cdot 10\text{H}_2\text{O}(\text{cr})$ and $\text{Na}_2\text{CaUO}_2(\text{CO}_3)_3 \cdot 6\text{H}_2\text{O}(\text{cr})$ must be used in combination with thermodynamic data for the binary $\text{U}(\text{VI})\text{--CO}_3$ and ternary $\text{Ca}\text{--U}(\text{VI})\text{--CO}_3$ aqueous species selected in the NEA-TDB (Guillaumont et al., 2003) and reported by Lee and Yun (2013), respectively. The use of other sources for the thermodynamic data of $\text{U}(\text{VI})$ carbonate aqueous species may result in inconsistencies and hence

Table 4

Solubility products of $\text{Ca}_2\text{UO}_2(\text{CO}_3)_3 \cdot 10\text{H}_2\text{O}(\text{cr})$ and $\text{Na}_2\text{CaUO}_2(\text{CO}_3)_3 \cdot 6\text{H}_2\text{O}(\text{cr})$ determined in the present work from experimental solubility data at room temperature at various ionic strength conditions (see text), compared with literature data.

Reactions	Background medium	$\log K'_{s,0}$	$\log K^{\circ}_{s,0}$	Ref.
$\text{Ca}_2\text{UO}_2(\text{CO}_3)_3 \cdot 10\text{H}_2\text{O}(\text{cr}) \rightleftharpoons 2\text{Ca}^{2+} + \text{UO}_2^{2+} + 3\text{CO}_3^{2-} + 10\text{H}_2\text{O}(\text{l})$	$\approx 0.03 \text{ m NaCl}$	$-(30.8 \pm 0.3)$	$-(32.4 \pm 0.3)$	p.w.
	0.51 m NaCl	$-(27.9 \pm 0.1)$	$-(32.2 \pm 0.1)$	p.w.
	0.1 m NaClO_4	$-(29.4 \pm 0.2)^a$	$-(32.3 \pm 0.2)$	p.w.
			$-(32.3 \pm 0.3)^b$	p.w.
			$-(30.3 \pm 1.0)$	$-(29.5 \pm 1.0)$ $-(32.1 \pm 1.0)$
$\text{Na}_2\text{CaUO}_2(\text{CO}_3)_3 \cdot 6\text{H}_2\text{O}(\text{cr}) \rightleftharpoons 2\text{Na}^+ + \text{Ca}^{2+} + \text{UO}_2^{2+} + 3\text{CO}_3^{2-} + 6\text{H}_2\text{O}(\text{l})$	5.61 m NaCl	$-(26.8 \pm 0.2)$	$-(31.8 \pm 0.5)$	p.w.
			$-(30.2 \pm 2.9)$	Alwan and Williams (1980)
		$-(29.0 \pm 2.9)$	$-(31.9 \pm 2.9)$	(Alwan and Williams, 1980), ^c

^a Average value from experimental data at $\text{pH}_m = 8.0$ and 8.3 .

^b Weighted average of $\log K^{\circ}_{s,0}$ determined from solubility experiments in $\approx 0.03 \text{ m NaCl}$, 0.51 m NaCl and 0.1 m NaClO_4 .

^c Re-calculated in the present work using solubility data reported in (Alwan and Williams, 1980) (see text).

large errors in the solubility calculations.

4.2. Implications of the newly derived thermodynamic data on the phase diagrams of the quaternary system Na–Ca–U(VI)–CO₃

New thermodynamic data derived in this work for $\text{Ca}_2\text{UO}_2(\text{CO}_3)_3 \cdot 10\text{H}_2\text{O}(\text{cr})$ and $\text{Na}_2\text{CaUO}_2(\text{CO}_3)_3 \cdot 6\text{H}_2\text{O}(\text{cr})$ in combination with thermodynamic data selected in the NEA–TDB (Guillaumont et al., 2003) or reported in the literature for other relevant U(VI) solid phases (Altmaier et al., 2005, 2017) are considered in this section to calculate phase diagrams for the ternary Ca–U(VI)–CO₃ and quaternary Na–Ca–U(VI)–CO₃ systems. Because of the number of variables affecting this system (*i.e.* pH , $a_{\text{Ca}^{2+}}$, a_{Na^+} , $a_{\text{HCO}_3^-}$) and the non-linear relationship among them, the diagrams $\log \{a_{\text{H}^+} \cdot a_{\text{HCO}_3^-}\}$ vs. $\log \{a_{\text{Ca}^{2+}} / (a_{\text{H}^+})^2\}$ (Fig. 4) and $\log \{a_{\text{Na}^+} / a_{\text{H}^+}\}$ vs. $\log \{a_{\text{Ca}^{2+}} / (a_{\text{H}^+})^2\}$ (Fig. 5a, b and c) with $\log \{a_{\text{H}^+} \cdot a_{\text{HCO}_3^-}\} = -8$, -10 and -12 have been chosen for the representation. These boundary conditions cover the stability fields of the most relevant solid phases in the quaternary system Na–Ca–U(VI)–CO₃.

The phase diagram for the ternary system Ca–U(VI)–CO₃ in Fig. 4 shows a large stability field for $\text{Ca}_2\text{UO}_2(\text{CO}_3)_3 \cdot 10\text{H}_2\text{O}(\text{cr})$ occurring at high $\log \{a_{\text{H}^+} \cdot a_{\text{HCO}_3^-}\}$ and high $\log \{a_{\text{Ca}^{2+}} / (a_{\text{H}^+})^2\}$. This field is however confined to a very narrow region by the precipitation of calcite above $y = 1.85 - x$ (with $x = \log \{a_{\text{Ca}^{2+}} / (a_{\text{H}^+})^2\}$ and $y = \log \{a_{\text{H}^+} \cdot a_{\text{HCO}_3^-}\}$) (dashed line in Fig. 4). This observation reflects a relevant feature for this system: in the absence of other major cations besides Ca, the solid phase $\text{Ca}_2\text{UO}_2(\text{CO}_3)_3 \cdot 10\text{H}_2\text{O}(\text{cr})$ will control the solubility of U(VI) in those systems saturated with calcite and with $\log \{a_{\text{Ca}^{2+}} / (a_{\text{H}^+})^2\}$ below ≈ 12 . However, Fig. 5a–c shows that the presence of Na importantly impacts the phase diagram of the quaternary system Na–Ca–U(VI)–CO₃, especially due to the formation of $\text{Na}_2\text{CaUO}_2(\text{CO}_3)_3 \cdot 6\text{H}_2\text{O}(\text{cr})$, $\text{Na}_4\text{UO}_2(\text{CO}_3)_3(\text{cr})$ and $\text{Na}_2\text{U}_2\text{O}_7 \cdot \text{H}_2\text{O}(\text{cr})$. A key feature of this system is the transition between $\text{Ca}_2\text{UO}_2(\text{CO}_3)_3 \cdot 10\text{H}_2\text{O}(\text{cr})$ and $\text{Na}_2\text{CaUO}_2(\text{CO}_3)_3 \cdot 6\text{H}_2\text{O}(\text{cr})$, which occurs at $\log \{a_{\text{Ca}^{2+}} / (a_{\text{Na}^+})^2\} \approx -(0.5 \pm 0.6)$. Note that the values of $\log \{a_{\text{H}^+} \cdot a_{\text{HCO}_3^-}\}$ considered in Fig. 5 cover those reported for seawater, granitic groundwaters, as well as clay (*e.g.* Callovo-Oxfordian, Opalinus clay), sedimentary and bentonite porewaters (Berner et al., 2013; Chester and Jickells, 2012; Gaucher et al., 2006; Grivé et al., 2010; Millero et al., 2008; Olmeda et al., 2017).

Fig. 5 highlights the complexity of the quaternary system Na–Ca–U(VI)–CO₃. High values of $\log \{a_{\text{H}^+} \cdot a_{\text{HCO}_3^-}\}$ promote the predominance of the ternary and quaternary solid phases $\text{Ca}_2\text{UO}_2(\text{CO}_3)_3 \cdot 10\text{H}_2\text{O}(\text{cr})$,

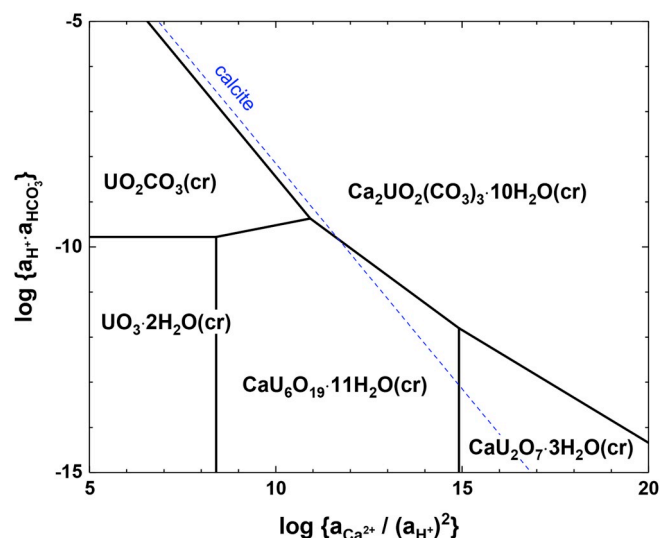


Fig. 4. Phase diagram for the ternary system Ca–U(VI)–CO₃ calculated using thermodynamic data derived in this work, selected in the NEA–TDB (Guillaumont et al., 2003), and reported by Altmaier and co-workers (Altmaier et al., 2005, 2017). Dashed line corresponds to the borderline for calcite precipitation.

$\text{Na}_2\text{CaUO}_2(\text{CO}_3)_3 \cdot 6\text{H}_2\text{O}(\text{cr})$ and $\text{Na}_4\text{UO}_2(\text{CO}_3)_3(\text{cr})$ (Fig. 5a), whereas $\text{Na}_2\text{U}_2\text{O}_7 \cdot \text{H}_2\text{O}(\text{cr})$ and $\text{CaU}_6\text{O}_{19} \cdot 11\text{H}_2\text{O}(\text{cr})$ become predominant at low $\log \{a_{\text{H}^+} \cdot a_{\text{HCO}_3^-}\}$ (Fig. 5c). Calcite precipitation is a key process that limits the formation of $\text{Ca}_2\text{UO}_2(\text{CO}_3)_3 \cdot 10\text{H}_2\text{O}(\text{cr})$ at $\log \{a_{\text{H}^+} \cdot a_{\text{HCO}_3^-}\} > -10$. The lower solubility of $\text{Na}_2\text{CaUO}_2(\text{CO}_3)_3 \cdot 6\text{H}_2\text{O}(\text{cr})$ (compared to $\text{Ca}_2\text{UO}_2(\text{CO}_3)_3 \cdot 10\text{H}_2\text{O}(\text{cr})$, see Fig. 1) leads to the formation of a predominance field for this solid phase at $\log \{a_{\text{H}^+} \cdot a_{\text{HCO}_3^-}\} > -12$ and before attaining calcite saturation.

The phase diagrams provided in this section can be used to evaluate/predict the solid phases controlling the solubility of uranium in the quaternary system Na–Ca–U(VI)–CO₃. These diagrams represent also a valuable tool for the design of future experiments dedicated to this system.

5. Summary and conclusions

The solubility and stability of liebigite was investigated in NaCl and NaClO₄ solutions with $0.03 \text{ m} \leq I_m \leq 5.61 \text{ m}$, $7 \leq \text{pH}_m \leq 9$ and

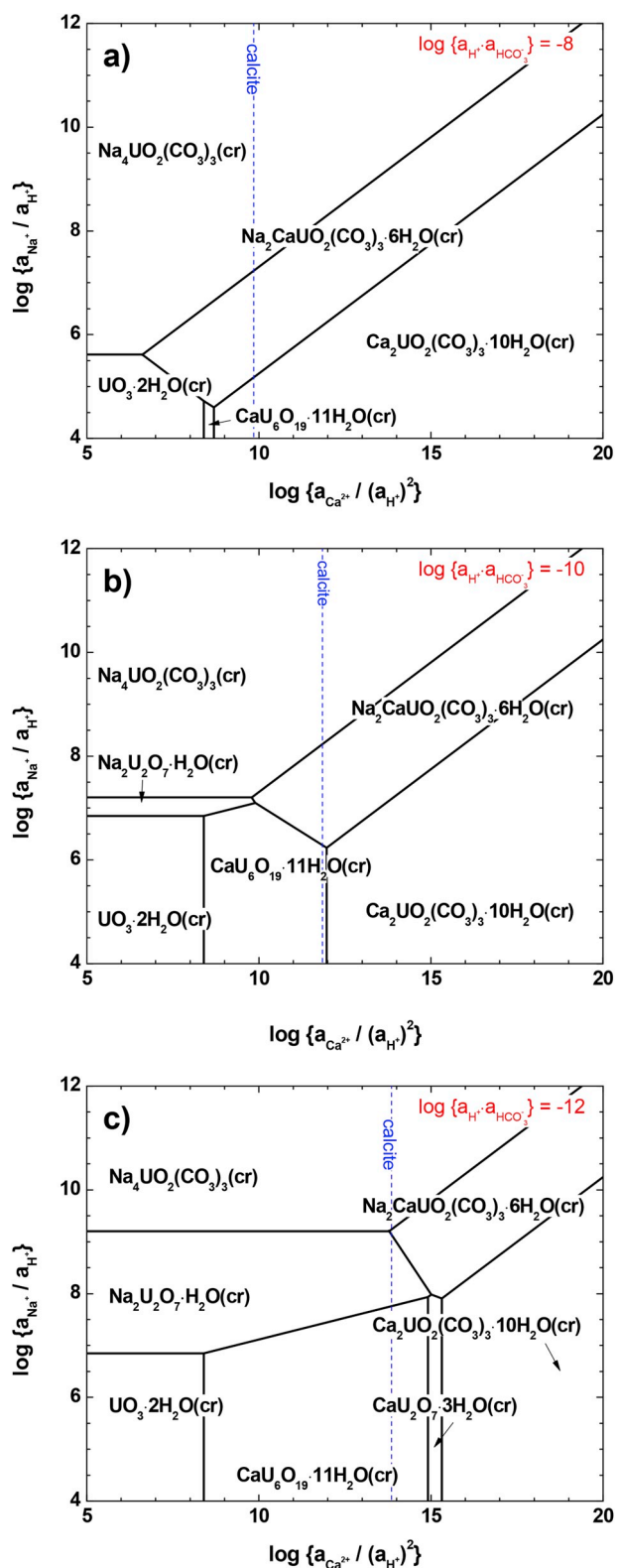


Fig. 5. Phase diagram for the quaternary system Na–Ca–U(VI)–CO₃ calculated for (a) $\log \{a_{\text{H}^+} \cdot a_{\text{HCO}_3^-}\} = -8$; (b) $\log \{a_{\text{H}^+} \cdot a_{\text{HCO}_3^-}\} = -10$; and (c) $\log \{a_{\text{H}^+} \cdot a_{\text{HCO}_3^-}\} = -12$, using thermodynamic data derived in this work, selected in the NEA–TDB (Guillaumont et al., 2003), and reported by Altmaier and co-workers (Altmaier et al., 2005, 2017). Dashed line corresponds to the borderline for calcite precipitation.

22 °C ≤ T ≤ 80 °C. The liebigite solid phase synthesized in this work was extensively characterized by XRD, quantitative chemical analysis, TG-DTA, SEM–EDS, IR and Raman spectroscopy. The information obtained with these techniques confirms the stoichiometry Ca₂UO₂(CO₃)₃·10H₂O(cr) for the starting material. The solubility of Ca₂UO₂(CO₃)₃·10H₂O(cr) at room temperature and I_m ≤ 0.51 m remains high ([U] ≈ 8–20 × 10⁻³ m) after attaining equilibrium conditions. The characterization of the solid phase after terminating the solubility experiments confirms the presence of Ca₂UO₂(CO₃)₃·10H₂O(cr), and thus that liebigite is the solid phase controlling the solubility of U(VI) in these conditions. This is consistent with the stoichiometric concentrations of uranium, calcium and carbonate measured in the aqueous phase, which confirm the congruent dissolution of the starting material. A significant drop in the solubility ([U] ≈ 8 × 10⁻⁵ m) is observed in 5.61 m solutions at T = 22 °C. XRD and quantitative chemical analysis confirm a complete transformation of liebigite to andersonite, Na₂CaUO₂(CO₃)₃·6H₂O(cr), under these conditions. A decrease in solubility in combination with a clear change in color of the U(VI) solid (from yellow to orange) suggest a solid phase transformation occurring in all investigated systems at T = 80 °C. This is further confirmed by XRD and quantitative chemical analysis, which support the destabilization of liebigite and predominance of uranate phases (CaU₂O₇·xH₂O(s), Na₂U₂O₇·xH₂O(s) and/or other sub-stoichiometric uranate compounds) in the investigated pH-range and temperature conditions.

Based on solubility data at room temperature determined in this work and considering the predominance of the binary/ternary complexes UO₂(CO₃)₃⁴⁻, CaUO₂(CO₃)₃²⁻ and Ca₂UO₂(CO₃)₃(aq) in the aqueous phase, the solubility products $\log K_{s,0}\{\text{Ca}_2\text{UO}_2(\text{CO}_3)_3 \cdot 10\text{H}_2\text{O}(\text{cr})\} = -(32.3 \pm 0.3)$ and $\log K_{s,0}\{\text{Na}_2\text{CaUO}_2(\text{CO}_3)_3 \cdot 6\text{H}_2\text{O}(\text{cr})\} = -(31.8 \pm 0.5)$ are derived. These results complement previously reported thermodynamic data for the system UO₂²⁺–Ca²⁺–Na⁺–H⁺–CO₂(g)–HCO₃⁻–CO₃²⁻–H₂O(l), thus allowing complete thermodynamic and geochemical calculations including U(VI) aqueous species and solid compounds of relevance in the environment and in the context of repositories for nuclear waste disposal.

Acknowledgements

The authors would like to thank Ezgi Yalçıntaş, Melanie Böttle, Frank Geyer, Cornelia Walschburger, Stephanie Kraft and Dieter Schild (all KIT–INE) for their scientific and technical support. Part of these experiments were performed in the context of a PhD thesis at the Technische Universität Dresden (S. Amayri). Robin Steudtner and Vinzenz Brendler (HZDR–IRE) are kindly acknowledged for organizing the transport of the liebigite used in this work. The scientific advice provided by Andrey Plyasunov (Russian Academy of Sciences) for the preparation of the phase diagrams is highly appreciated. This study was partly funded by the German Ministry of Economic Affairs and Energy (BMWi) (EDUKEM project, contract number 02E11334) and by the German Federal Ministry for Education and Research (BMBF) (ThermAc project, contract number 02NUK039A).

Appendix A. Supplementary data

Supplementary data to this article can be found online at <https://doi.org/10.1016/j.apgeochem.2019.104374>.

Appendix

Table A-1

Chemical thermodynamic data at $I = 0$ considered in the present work (p.w.) for thermodynamic calculations, and used in Alwan and Williams (1980) to calculate the aqueous speciation of uranium.

Reactions	$\log \beta^\circ$	
	p.w.	Alwan and Williams (Alwan and Williams, 1980)
$\text{H}_2\text{CO}_3^* \rightleftharpoons \text{HCO}_3^- + \text{H}^+$	-6.35 ^a	-6.379 ^b
$\text{HCO}_3^- \rightleftharpoons \text{H}^+ + \text{CO}_3^{2-}$	-10.33 ^a	-10.33 ^b
$\text{Na}^+ + \text{HCO}_3^- \rightleftharpoons \text{NaHCO}_3(\text{aq})$	-	-0.250 ^b
$\text{Na}^+ + \text{CO}_3^{2-} \rightleftharpoons \text{NaCO}_3^-$	-	1.268 ^b
$2\text{Na}^+ + \text{CO}_3^{2-} \rightleftharpoons \text{Na}_2\text{CO}_3(\text{aq})$	-	0.672 ^b
$\text{Ca}^{2+} + \text{HCO}_3^- \rightleftharpoons \text{CaHCO}_3^+$	1.10 ^a	1.26 ^b
$\text{Ca}^{2+} + \text{CO}_3^{2-} \rightleftharpoons \text{CaCO}_3(\text{aq})$	3.22 ^a	3.2 ^b
$\text{Ca}^{2+} + \text{H}_2\text{O}(\text{l}) \rightleftharpoons \text{CaOH}^+ + \text{H}^+$	-12.78 ^a	-12.85 ^c
$\text{Ca}^{2+} + 2\text{H}_2\text{O}(\text{l}) \rightleftharpoons \text{Ca}(\text{OH})_2(\text{aq}) + 2\text{H}^+$	-30 ^d	-
$\text{UO}_2^{2+} + \text{H}_2\text{O}(\text{l}) \rightleftharpoons \text{UO}_2\text{OH}^+ + \text{H}^+$	$(-5.25 \pm 0.24)^e$	-5.8 ^c
$\text{UO}_2^{2+} + 2\text{H}_2\text{O}(\text{l}) \rightleftharpoons \text{UO}_2(\text{OH})_2(\text{aq}) + 2\text{H}^+$	$(-12.15 \pm 0.07)^e$	-
$\text{UO}_2^{2+} + 3\text{H}_2\text{O}(\text{l}) \rightleftharpoons \text{UO}_2(\text{OH})_3^- + 3\text{H}^+$	$(-20.7 \pm 0.40)^f$	-
$\text{UO}_2^{2+} + 4\text{H}_2\text{O}(\text{l}) \rightleftharpoons \text{UO}_2(\text{OH})_4^{2-} + 4\text{H}^+$	$(-31.9 \pm 0.2)^f$	-
$2\text{UO}_2^{2+} + 2\text{H}_2\text{O}(\text{l}) \rightleftharpoons (\text{UO}_2)_2(\text{OH})_2^{2+} + 2\text{H}^+$	$(-5.62 \pm 0.04)^e$	-5.62 ^c
$3\text{UO}_2^{2+} + 4\text{H}_2\text{O}(\text{l}) \rightleftharpoons (\text{UO}_2)_3(\text{OH})_4^{2+} + 4\text{H}^+$	$(-11.90 \pm 0.30)^e$	-11.75 ^c
$3\text{UO}_2^{2+} + 5\text{H}_2\text{O}(\text{l}) \rightleftharpoons (\text{UO}_2)_3(\text{OH})_5^+ + 5\text{H}^+$	$(-15.55 \pm 0.12)^e$	-15.63 ^c
$3\text{UO}_2^{2+} + 7\text{H}_2\text{O}(\text{l}) \rightleftharpoons (\text{UO}_2)_3(\text{OH})_7^- + 7\text{H}^+$	$(-32.20 \pm 0.80)^e$	-
$4\text{UO}_2^{2+} + 7\text{H}_2\text{O}(\text{l}) \rightleftharpoons (\text{UO}_2)_4(\text{OH})_7^+ + 7\text{H}^+$	$(-21.90 \pm 1.00)^e$	-
$\text{UO}_2^{2+} + \text{CO}_3^{2-} \rightleftharpoons \text{UO}_2\text{CO}_3(\text{aq})$	$(9.94 \pm 0.03)^e$	10.1 ^g
$\text{UO}_2^{2+} + 2\text{CO}_3^{2-} \rightleftharpoons \text{UO}_2(\text{CO}_3)_2^{2-}$	$(16.61 \pm 0.09)^e$	17.1 ^g
$\text{UO}_2^{2+} + 3\text{CO}_3^{2-} \rightleftharpoons \text{UO}_2(\text{CO}_3)_3^{4-}$	$(21.84 \pm 0.04)^e$	21.4 ^g
$3\text{UO}_2^{2+} + 6\text{CO}_3^{2-} \rightleftharpoons (\text{UO}_2)_3(\text{CO}_3)_6^{6-}$	$(54.00 \pm 1.00)^e$	-
$\text{Ca}^{2+} + \text{UO}_2^{2+} + 3\text{CO}_3^{2-} \rightleftharpoons \text{CaUO}_2(\text{CO}_3)_3^{2-}$	$(27.27 \pm 0.14)^h$	-
$2\text{Ca}^{2+} + \text{UO}_2^{2+} + 3\text{CO}_3^{2-} \rightleftharpoons \text{Ca}_2\text{UO}_2(\text{CO}_3)_3(\text{aq})$	$(29.81 \pm 0.19)^h$	-
Solubility product	$\log K_{s,0}^\circ$	
	p.w.	Alwan and Williams (Alwan and Williams, 1980)
$\text{CaCO}_3(\text{s}) \rightleftharpoons \text{Ca}^{2+} + \text{CO}_3^{2-}$	-8.48 ^a	-
$\text{UO}_3 \cdot 2\text{H}_2\text{O}(\text{cr}) + 2\text{H}^+ \rightleftharpoons \text{UO}_2^{2+} + 3\text{H}_2\text{O}(\text{l})$	$(5.35 \pm 0.13)^f$	-
$0.5\text{Na}_2\text{U}_2\text{O}_7 \cdot \text{H}_2\text{O}(\text{cr}) + 3\text{H}^+ \rightleftharpoons \text{Na}^+ + \text{UO}_2^{2+} + 2\text{H}_2\text{O}(\text{l})$	$(12.2 \pm 0.2)^f$	-
$0.5\text{CaU}_2\text{O}_7 \cdot 3\text{H}_2\text{O}(\text{cr}) + 3\text{H}^+ \rightleftharpoons 0.5\text{Ca}^{2+} + \text{UO}_2^{2+} + 4\text{H}_2\text{O}(\text{l})$	$(11.7 \pm 0.5)^i$	-
$\text{CaU}_6\text{O}_{19} \cdot 11\text{H}_2\text{O}(\text{cr}) + 14\text{H}^+ \rightleftharpoons \text{Ca}^{2+} + 6\text{UO}_2^{2+} + 18\text{H}_2\text{O}(\text{l})$	$(40.50 \pm 1.60)^e$	-
$\text{UO}_2\text{CO}_3(\text{cr}) \rightleftharpoons \text{UO}_2^{2+} + \text{CO}_3^{2-}$	$(-14.76 \pm 0.02)^e$	-
$\text{Na}_4\text{UO}_2(\text{CO}_3)_3(\text{cr}) \rightleftharpoons 4\text{Na}^+ + \text{UO}_2^{2+} + 3\text{CO}_3^{2-}$	$(-27.18 \pm 0.16)^e$	-

a. (Giffaut et al., 2014); b. (Truesdell and Jones, 1974); c. (Baes and Mesmer, 1976); d. (Stumm and Morgan, 1996); e. (Guillaumont et al., 2003); f. (Altmaier et al., 2017); g. (Langmuir, 1978); h. (Lee and Yun, 2013); i. (Altmaier et al., 2005).

Table A-2

SIT interaction coefficients (ϵ) of main aqueous species used for ionic strength corrections in this work.

Chemical species	$\epsilon(i, \text{Na}^+) (\text{kg}\cdot\text{mol}^{-1})$	$\epsilon(j, \text{Cl}^-) (\text{kg}\cdot\text{mol}^{-1})$	$\epsilon(j, \text{ClO}_4^-) (\text{kg}\cdot\text{mol}^{-1})$
H^+	-	$(0.12 \pm 0.01)^a$	$(0.14 \pm 0.02)^a$
UO_2^{2+}	-	$(0.21 \pm 0.02)^a$	$(0.46 \pm 0.03)^a$
Ca^{2+}	-	$(0.14 \pm 0.01)^a$	$(0.27 \pm 0.03)^a$
OH^-	$(0.04 \pm 0.01)^a$	-	-
HCO_3^-	$(0.00 \pm 0.02)^a$	-	-
CO_3^{2-}	$(-0.08 \pm 0.03)^a$	-	-
CaHCO_3^+	-	$(0.05 \pm 0.10)^b$	$(0.20 \pm 0.10)^b$
UO_2OH^+	-	$(0.10 \pm 0.10)^c$	$(-0.06 \pm 0.40)^a$
$\text{UO}_2(\text{OH})_3^-$	$(-0.24 \pm 0.09)^c$	-	-
$\text{UO}_2(\text{OH})_4^{2-}$	$(0.01 \pm 0.04)^c$	-	-
$(\text{UO}_2)_2(\text{OH})_2^{2+}$	-	$(0.30 \pm 0.06)^c$	$(0.57 \pm 0.07)^a$
$(\text{UO}_2)_3(\text{OH})_4^{2+}$	-	$(-0.07 \pm 0.17)^c$	$(0.89 \pm 0.23)^a$
$(\text{UO}_2)_3(\text{OH})_5^+$	-	$(0.24 \pm 0.15)^c$	$(0.45 \pm 0.15)^a$
$(\text{UO}_2)_3(\text{OH})_7^-$	$(-0.24 \pm 0.09)^c$	-	-
$(\text{UO}_2)_4(\text{OH})_7^+$	-	$(0.17 \pm 0.18)^c$	$(0.45 \pm 0.15)^d$
$\text{UO}_2(\text{CO}_3)_2^{2-}$	$(-0.02 \pm 0.09)^a$	-	-
$\text{UO}_2(\text{CO}_3)_3^{4-}$	$(-0.01 \pm 0.11)^a$	-	-

(continued on next page)

Table A-2 (continued)

Chemical species	$\varepsilon(i, \text{Na}^+)$ (kg·mol ⁻¹)	$\varepsilon(j, \text{Cl}^-)$ (kg·mol ⁻¹)	$\varepsilon(j, \text{ClO}_4^-)$ (kg·mol ⁻¹)
(UO ₂) ₃ (CO ₃) ₆ ⁶⁻	(0.37 ± 0.11) ^a	-	-
(UO ₂) ₂ (CO ₃) ₃ (OH) ₃ ⁻	(0.00 ± 0.05) ^b	-	-
CaUO ₂ (CO ₃) ₃ ²⁻	-(0.02 ± 0.09) ^c	-	-

a. (Grenthe et al., 2013); b. Estimated by charge analogy as described in Hummel (2009) (Hummel, 2009); c. (Altmaier et al., 2017); d. In analogy with $\varepsilon((\text{UO}_2)_3(\text{OH})_5^+, \text{ClO}_4^-)$ selected in the NEA-TDB; e. In analogy with $\varepsilon(\text{UO}_2(\text{CO}_3)_2^{2-}, \text{Na}^+)$ selected in the NEA-TDB.

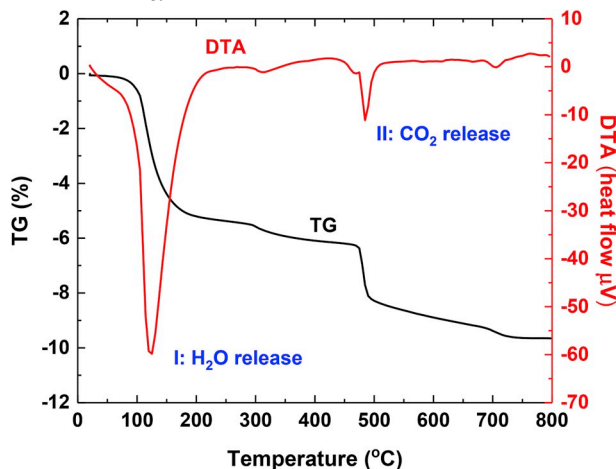


Figure A-1. TG and DTA data obtained for the starting Ca₂UO₂(CO₃)₃·10H₂O(cr) solid used in this work.

Table A-3

Results of the thermogravimetric analysis conducted for the starting Ca₂UO₂(CO₃)₃·10H₂O(cr) solid used in this work.

Step	Temperature (°C)			Mass - DM (%)	Release of H ₂ O or CO ₂ (mol)
	T _{initial}	T _{peak}	T _{final}		
1 - endothermic	21.8		45.7		Humidity
2 - endothermic	45.7	121.5	246.1	24.85	10.07 H ₂ O
3 - endothermic	246.1	309.9	420.4	3.96	0.65 CO ₂
4 - endothermic	420.4	481.7	625.5	13.61	2.26 CO ₂
5 - endothermic	625.5	702.1	800.1	3.12	0.52 CO ₂
Σ	21.8		800.1	45.54	Remaining Ca ₂ UO ₅ = 54.46%

Table A-4

Saturation index of calcite calculated for the experimental conditions in the present work. Calculations performed using thermodynamic data summarized in Tables A-1 and A-2.

Background medium	SI of calcite
≈ 0.03 m NaCl	0.4
0.51 m NaCl	0
0.1 m NaClO ₄	0.3
5.61 m NaCl	-0.6

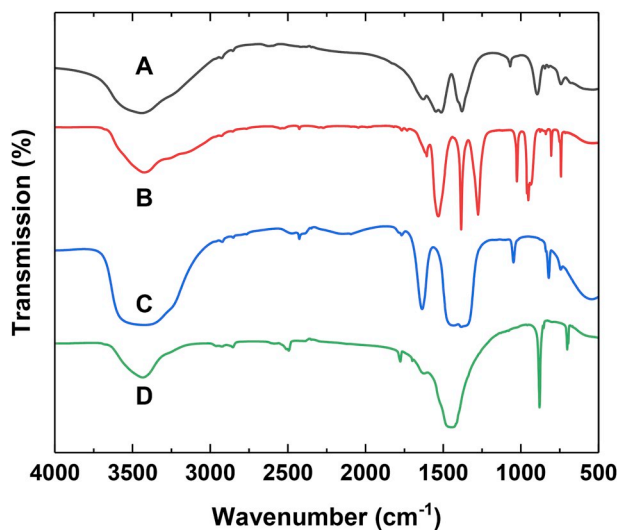


Figure A-2. IR spectra of the starting $\text{Ca}_2\text{UO}_2(\text{CO}_3)_3 \cdot 10\text{H}_2\text{O}(\text{cr})$ solid (A), and the chemical reagents used in its synthesis: $\text{UO}_2(\text{NO}_3)_2 \cdot 6\text{H}_2\text{O}$ (B), $\text{Ca}(\text{NO}_3)_2 \cdot 4\text{H}_2\text{O}$ (C) and Na_2CO_3 (D).

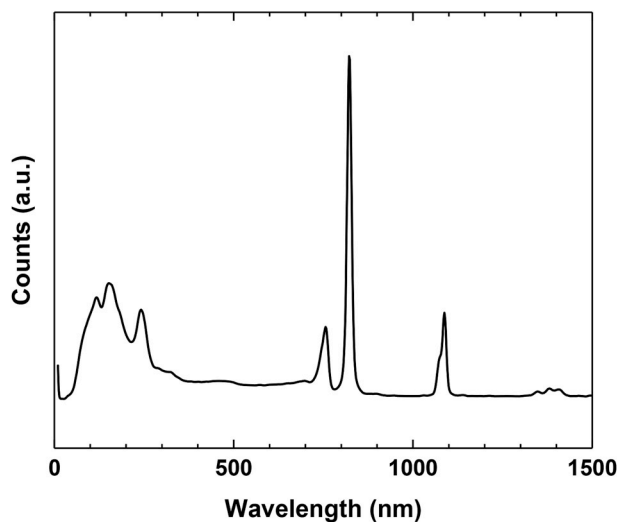


Figure A-3. Raman spectra collected for the starting $\text{Ca}_2\text{UO}_2(\text{CO}_3)_3 \cdot 10\text{H}_2\text{O}(\text{cr})$ solid used in this work.

References

- Altmaier, M., Gaona, X., Fanghänel, T., 2013. Recent advances in aqueous actinide chemistry and thermodynamics. *Chem. Rev.* 113, 901–943.
- Altmaier, M., Metz, V., Neck, V., Müller, R., Fanghänel, T., 2003. Solid-liquid equilibria of $\text{Mg}(\text{OH})_2(\text{cr})$ and $\text{Mg}_2(\text{OH})_3\text{Cl} \cdot 4\text{H}_2\text{O}(\text{cr})$ in the system $\text{Mg}-\text{Na}-\text{H}-\text{OH}-\text{Cl}-\text{H}_2\text{O}$ at 25°C. *Geochem. Cosmochim. Acta* 67, 3595–3601.
- Altmaier, M., Neck, V., Müller, R., Fanghänel, T., 2005. Solubility of U(VI) and formation of $\text{CaU}_2\text{O}_7 \cdot 3\text{H}_2\text{O}(\text{cr})$ in alkaline CaCl_2 solutions. In: *International Conference on Chemistry and Migration Behaviour of Actinides and Fission Products in the Geosphere*. Avignon, France.
- Altmaier, M., Yalçıntaş, E., Gaona, X., Neck, V., Müller, R., Schlieker, M., Fanghänel, T., 2017. Solubility of U(VI) in chloride solutions. I. The stable oxides/hydroxides in NaCl systems, solubility products, hydrolysis constants and SIT coefficients. *J. Chem. Thermodyn.* 114, 2–13.
- Alwan, A.K., Williams, P.A., 1980. The aqueous chemistry of uranium minerals. Part 2. Minerals of the liebigite group. *Mineral. Mag.* 43, 665–667.
- Amayri, S., 2002. Synthese, Charakterisierung und Löslichkeit von Erdalkaliuranylcarbonaten $\text{M}_2[\text{UO}_2(\text{CO}_3)_3] \cdot x\text{H}_2\text{O}$; M: Mg, Ca, Sr, Ba, Fakultät Mathematik und Naturwissenschaften. Tech. Univ. Dresd., FZR-359 Dresden.
- Amayri, S., Arnold, T., Reich, T., Foerstendorf, H., Geipel, G., Bernhard, G., Massanek, A., 2004. Spectroscopic characterization of the uranium carbonate andersonite $\text{Na}_2\text{Ca}[\text{UO}_2(\text{CO}_3)_3] \cdot 6\text{H}_2\text{O}$. *Environ. Sci. Technol.* 38, 6032–6036.
- Baes, C.F., Mesmer, R.E., 1976. *The Hydrolysis of Cations*. Wiley, New York.
- Beccia, M.R., Matara-Aho, M., Reeves, B., Roques, J., Solari, P.L., Monfort, M., Moulin, C., Den Auwer, C., 2017. New insight into the ternary complexes of uranyl carbonate in seawater. *J. Environ. Radioact.* 178–179, 343–348.
- Berner, U., Kulik, D.A., Kosakowski, G., 2013. Geochemical impact of a low-pH cement liner on the near field of a repository for spent fuel and high-level radioactive waste. *Phys. Chem. Earth, Parts A/B/C* 64, 46–56.
- Bernhard, G., Geipel, G., Brendler, V., Nitsche, H., 1996. Speciation of uranium in seepage waters of a mine tailing pile studied by time-resolved laser-induced fluorescence spectroscopy (TRLFS). *Radiochim. Acta* 74, 87–91.
- Bernhard, G., Geipel, G., Reich, T., Brendler, V., Amayri, S., Nitsche, H., 2001. Uranyl(VI) carbonate complex formation: validation of the $\text{Ca}_2\text{UO}_2(\text{CO}_3)_3(\text{aq.})$ species. *Radiochim. Acta* 89, 511–518.
- Cejka, J., Urbanec, Z., 1999. Infrared spectroscopy and thermal analysis of the uranyl minerals. *Rev. Mineral. Geochem.* 38, 521–622.
- Çevirim-Papaioannou, N., Yalçıntaş, E., Gaona, X., Altmaier, M., Geckeis, H., 2018a. Solubility of U(VI) in chloride solutions. II. The stable oxides/hydroxides in alkaline KCl solutions: thermodynamic description and relevance in cementitious systems. *Appl. Geochem.* 98, 237–246.
- Çevirim-Papaioannou, N., Yalçıntaş, E., Gaona, X., Dardenne, K., Altmaier, M., Geckeis, H., 2018b. Redox chemistry of uranium in reducing, dilute to concentrated NaCl solutions. *Appl. Geochem.* 98, 286–300.
- Chernorukov, N.G., Knyazev, A.V., Vlasova, E.V., Kuznetsova, N.Y., 2009. A physico-chemical study of alkaline-earth metal carbonatouranylates. *Radiochemistry* 51, 244–249.
- Chester, R., Jickells, T., 2012. *Marine Geochemistry*, 3 ed. Wiley-Blackwell, West Sussex.
- Choi, B.-Y., Kim, G.-Y., Koh, Y.-K., Shin, S.-H., Yoo, S.-W., Kim, D.-H., 2008. Geochemical characteristics of a LILW repository I. Groundwater. *J. Korean Radioact. Waste Soc.* 6, 297–306.
- Ciavatta, L., 1980. The specific interaction theory in evaluating ionic equilibria. *Ann. Chim.* 70, 551–567.
- Dong, W., Brooks, S.C., 2006. Determination of the formation constants of ternary complexes of uranyl and carbonate with alkaline earth metals (Mg^{2+} , Ca^{2+} , Sr^{2+} , and Ba^{2+}) using anion exchange method. *Environ. Sci. Technol.* 40, 4689–4695.

- Endrizzi, F., Gaona, X., Marques Fernandes, M., Baeyens, B., Altmair, M., 2018. Solubility and hydrolysis of U(VI) in 0.5 mol/kg NaCl solutions at T = 22 and 80 °C. *J. Chem. Thermodyn.* 120, 45–53.
- Endrizzi, F., Leggett, C.J., Rao, L., 2016. Scientific basis for efficient extraction of uranium from seawater. I: understanding the chemical speciation of uranium under seawater conditions. *Ind. Eng. Chem. Res.* 55, 4249–4256.
- Endrizzi, F., Rao, L., 2014. Chemical speciation of uranium(VI) in marine environments: complexation of calcium and magnesium ions with $[(\text{UO}_2)(\text{CO}_3)_3]^{4-}$ and the effect on the extraction of uranium from seawater. *Chem. Eur J.* 20, 14499–14506.
- Fox, P.M., Davis, J.A., Zachara, J.M., 2006. The effect of calcium on aqueous uranium(VI) speciation and adsorption to ferrihydrite and quartz. *Geochem. Cosmochim. Acta* 70, 1379–1387.
- Gaona, X., Fellhauer, D., Altmair, M., 2013. Thermodynamic description of Np(VI) solubility, hydrolysis, and redox behavior in dilute to concentrated alkaline NaCl solutions. *Pure Appl. Chem.* 85, 2027–2049.
- Gaucher, É.C., Blanc, P., Bardot, F., Braibant, G., Buschaert, S., Crouzet, C., Gautier, A., Girard, J.-P., Jacquot, E., Lassin, A., Negrel, G., Tournassat, C., Vinsot, A., Altmann, S., 2006. Modelling the porewater chemistry of the Callovian–Oxfordian formation at a regional scale. *Compt. Rendus Geosci.* 338, 917–930.
- Geipel, G., Amayri, S., Bernhard, G., 2008. Mixed complexes of alkaline earth uranyl carbonates: a laser-induced time-resolved fluorescence spectroscopic study. *Spectrochim. Acta, Part A* 71, 53–58.
- Giffaut, E., Grivé, M., Blanc, P., Vieillard, P., Colàs, E., Gailhanou, H., Gaboreau, S., Marty, N., Madé, B., Duro, L., 2014. Andra thermodynamic database for performance assessment: ThermoChimie. *Appl. Geochem.* 49, 225–236.
- Gordon, L.I., Jones, L.B., 1973. The effect of temperature on carbon dioxide partial pressures in seawater. *Mar. Chem.* 1, 317–322.
- Gorman-Lewis, D., Burns, P.C., Fein, J.B., 2008. Review of uranyl mineral solubility measurements. *J. Chem. Thermodyn.* 40, 335–352.
- Grenthe, I., Mompean, F., Spahiu, K., Wanner, H., 2013. Guidelines for the Extrapolation to Zero Ionic Strength. OECD-NEA, Paris.
- Grivé, M., Domènech, C., Montoya, V., García, D., Duro, L., 2010. Determination and Assessment of the Concentration Limits to Be Used in SR-Can. SKB.
- Guillaumont, R., Fanghänel, T., Neck, V., Fuger, J., Palmer, D.A., Grenthe, I., Rand, M.H., 2003. Update on the Chemical Thermodynamics of Uranium, Neptunium, Plutonium, Americium and Technetium. Elsevier; OECD-NEA, Amsterdam.
- Hummel, W., 2009. Ionic strength corrections and estimation of SIT ion interaction coefficients. PSI, TM-44-09-01.
- Jo, Y., Lee, J.-Y., Yun, J.-I., 2018. Adsorption of uranyl tricarbonate and calcium uranyl carbonate onto γ -alumina. *Appl. Geochem.* 94, 28–34.
- Langmuir, D., 1978. Uranium solution-mineral equilibria at low temperatures with applications to sedimentary ore deposits. *Geochem. Cosmochim. Acta* 42, 547–569.
- Lee, J.-Y., Vespa, M., Gaona, X., Dardenne, K., Rothe, J., Rabung, T., Altmair, M., Yun, J.-I., 2017. Formation, stability and structural characterization of ternary $\text{Mg}_2\text{UO}_2(\text{CO}_3)_3^{2-}$ and $\text{Mg}_2\text{UO}_2(\text{CO}_3)_3(\text{aq})$ complexes. *Radiochim. Acta* 105, 171–185.
- Lee, J.-Y., Yun, J.-I., 2013. Formation of ternary $\text{CaUO}_2(\text{CO}_3)_3^{2-}$ and $\text{Ca}_2\text{UO}_2(\text{CO}_3)_3(\text{aq})$ complexes under neutral to weakly alkaline conditions. *Dalton Trans.* 42, 9862–9869.
- Maia, F., Grivé, M., Madé, B., Montavon, G., 2017. Impact of Temperature on U(VI) Sorption by Callovo-Oxfordian Clay Rock, International Conference on Chemistry and Migration Behaviour of Actinides and Fission Products in the Geosphere. pp. 303–304 Barcelona.
- Maloubier, M., Solari, P.L., Moisy, P., Monfort, M., Den Auwer, C., Moulin, C., 2015. XAS and TR-LIF spectroscopy of uranium and neptunium in seawater. *Dalton Trans.* 44, 5417–5427.
- Meyrowitz, R., Ross, D.R., Weeks, A.D., 1963. Synthesis of Liebigite. U. S. Geological Survey Professional Papers Nr. 475-B, pp. 162–163.
- Millero, F.J., Feistel, R., Wright, D.G., McDougall, T.J., 2008. The composition of standard seawater and the definition of the reference-composition salinity scale. *Deep Sea Res. Part I* 55, 50–72.
- Neck, V., Altmair, M., Rabung, T., Lützenkirchen, J., Fanghänel, T., 2009. Thermodynamics of trivalent actinides and neodymium in NaCl, MgCl_2 , and CaCl_2 solutions: solubility, hydrolysis, and ternary Ca-M(III)-OH complexes. *Pure Appl. Chem.* 81, 1555–1568.
- Olmeda, J., Henocq, P., Giffaut, E., Grivé, M., 2017. Modelling of chemical degradation of blended cement-based materials by leaching cycles with Callovo-Oxfordian porewater. *Phys. Chem. Earth, Parts A/B/C* 99, 110–120.
- Prat, O., Vercouter, T., Ansoborlo, E., Fichet, P., Perret, P., Kurtio, P., Salonen, L., 2009. Uranium speciation in drinking water from drilled wells in southern Finland and its potential links to health effects. *Environ. Sci. Technol.* 43, 3941–3946.
- Saleh, A.S., Lee, J.-Y., Jo, Y., Yun, J.-I., 2018. Uranium(VI) sorption complexes on silica in the presence of calcium and carbonate. *J. Environ. Radioact.* 182, 63–69.
- Seder-Colomina, M., Mangeret, A., Stetten, L., Merrot, P., Diez, O., Julien, A., Barker, E., Thouvenot, A., Bargar, J., Cazala, C., Morin, G., 2018. Carbonate facilitated mobilization of uranium from lacustrine sediments under anoxic conditions. *Environ. Sci. Technol.* 52, 9615–9624.
- Stumm, W., Morgan, J.J., 1996. *Aquatic Chemistry*, 3 ed. John Wiley & Sons, New York.
- Truesdell, A.H., Jones, B.F., 1974. WATEQ, A computer program for calculating chemical equilibrium of natural waters. *J. Res. U. S. Geol. Surv.* 2, 233–248.
- Urbanec, Z., Cejka, J., 1979. Infrared spectra of liebigite, andersonite, voglite, and schroëckingerite. *Collect. Czechoslov. Chem. Commun.* 44, 10–23.
- Vochten, R., van Haverbeke, L., van Springel, K., 1993. Synthesis of liebigite and andersonite, and study of their thermal behavior and luminescence. *Can. Mineral.* 31, 167–171.
- Yalçıntaş, E., Gaona, X., Altmair, M., Dardenne, K., Polly, R., Geckeis, H., 2016. Thermodynamic description of Tc(IV) solubility and hydrolysis in dilute to concentrated NaCl, MgCl_2 and CaCl_2 solutions. *Dalton Trans.* 45, 8916–8936.